

5 TRACKING AND ALIGNMENT

During first pp production run the HADES spectrometer was equipped for the first time with an almost complete outer tracking system (four MDC chambers in four sectors, three chambers in the remaining two sectors).

One of the main goal of this experiment was to collect data with pp elastic scattering, in order to perform a full characterization of the tracking system, to check and improve the alignment of the chambers, and in particular to evaluate momentum reconstruction resolution.

Indeed a high momentum resolution is mandatory to do exclusive η identification, which requires precise MDC calibration and detector alignment. For this purpose several alignment procedures have to be developed, and tracking algorithms which reconstruct momentum by using even the information coming from the outer chambers.

In this chapter it will be presented the status of HADES tracking precision, evaluated in January 2004 experimental data.

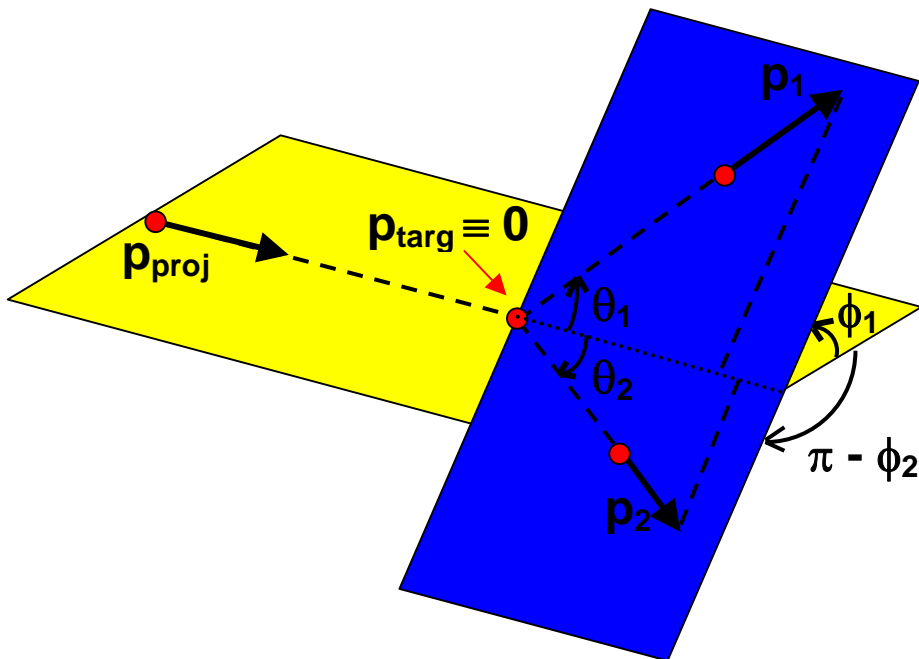


Figure 5.1 – Scheme of a two-body collision in the laboratory frame.

5.1 Elastic kinematics

The pp elastic channel is a wonderful tool to study the detector alignment and its tracking capability. Indeed in elastic scattering the kinematics of the reaction is fixed, and so the relationship between angular variables of proton pairs is well fixed. From the information of the polar angle is even possible to have an estimation of the particle momentum, and so to evaluate the momentum reconstruction resolution.

Figure 5.1 shows a scheme of a two-body collision, like pp elastic scattering, in the laboratory frame. In the figure we have a projectile with momentum p_{proj} hitting the

target particle which is at rest frame ($p_{\text{targ}} \equiv 0$). After the collision the two outgoing particles will be emitted in the same reaction plane (the blue one), with emission polar angles θ_1 and θ_2 and with momenta p_1 and p_2 ; the two particles are identical so it is not possible to distinguish projectile and target after the collision.

The first kinematical constraint comes from the fact the two particle trajectories must lay on the same reaction plane, and it imposes the condition on azimuthal angles (ϕ_1 and ϕ_2):

$$|\phi_1 - \phi_2| = 180^\circ \quad (\text{Eq. 5-1})$$

Furthermore, considering that the two particles have the same rest mass, from relativistic calculation it is possible to find the relationship between their polar angles (θ_1 and θ_2):

$$\tan \theta_1 \cdot \tan \theta_2 = \frac{1}{\gamma_{CM}^2} \quad (\text{Eq. 5-2})$$

where γ_{CM} is the γ Lorentz factor calculated in the centre of mass frame.

In elastic scattering there is a direct relationship between emission angle and particle momentum; by doing some other relativistic calculations we can obtain:

$$p(\theta) = \frac{P_{proj}}{\cos \theta + \gamma_{CM}^2 \sin \theta \cos \theta} \quad (\text{Eq. 5-3})$$

From the last equation, if we are able to measure correctly the θ polar angle, we can predict the theoretical momentum the particle should have, and to compare this value with the one given by tracking algorithms. In this way we can estimate momentum resolution of the tracking system.

But the main purpose of the HADES spectrometer is to plot invariant mass spectra of dilepton pairs, so we are interested much more in invariant mass resolution respect to momentum one.

In relativistic notation, we can express the four-momentum p_i of a particle such as:

$$p_i = (E_i, \vec{p}_i); \quad E_i = \sqrt{p_i^2 + m^2} \quad (\text{Eq. 5-4})$$

where E_i is the total energy of the particle, \vec{p}_i its momentum vector and m its rest mass. If we have a system made by two particles, their invariant mass M will be given by:

$$M = \sqrt{(E_1 + E_2)^2 - (\vec{p}_1 + \vec{p}_2)^2} \quad (\text{Eq. 5-5})$$

If we are able to select a proton elastic pair, measuring the particle momenta and angular variables we can estimate its invariant mass, and compare the obtained value with the initial state one.

Table 5-1 shows a summary of the kinematical properties of proton elastic scattering pairs, for the two energies which were used in January 2004 experiment.

No field data were taken at a proton incident kinetic energy of 2 GeV, to perform alignment using straight tracks, while the field data were taken at 2.2 GeV.

	No field	Field
Momentum (proj) [MeV/c]	2784	3000
Total energy (proj) [MeV]	2938	3143
Kinetic energy (proj) [MeV]	2000	2205
Invariant mass [MeV/c ²]	2697	2768
γ_{CM}	1.4372	1.4747
$1/\gamma_{CM}^2$	0.4841	0.4598

Table 5-1 – Summary of the kinematical properties of proton elastic scattering

5.2 Alignment strategy

Each MDC chamber provides an information about the position and the trajectory direction of the particle which hit it, in the chamber coordinate frame¹, by fitting time signals coming from different wire layers.

The particle trajectory before and after the magnetic field is reconstructed by spatial correlation of different chambers belonging to the same sector, and after the particle momentum is evaluated. In this case the position information of the single MDC needs to be converted into the laboratory coordinate system, and it is important to know the absolute position of each chamber with high precision to obtain high precision in the trajectory reconstruction.

We have developed alignment procedures based on photometric measurement and cosmic data for the inner chambers, and on straight track reconstruction in run without magnetic field for the outer ones.

Photometry is a photo-camera based method to survey objects in three dimensions. For this purpose a 8 Megapixel mirror reflex camera with a special 20 mm USM wide-angle-lens was used, to make high resolution pictures of large areas from short distances.

First the camera has to be calibrated, by photographing from all sides a special array of dots whose positions are fixed and known. After some special markers are glued on the chambers, in detector reference positions. The software can make a fit to

¹ The chamber coordinate frame is defined by the middle plane of each chamber (xy plane) and its central point (origin).

the marker pattern and then calculates the centre of gravity in sub-pixel precision. By this procedure we are able to calculate the position and rotation parameters of each chamber.

For January 2004 experimental run the photometric method was used for inner chambers. First photos were made on MDC II chambers and the magnet support structure and then, after moving plane I to measuring position, the same for MDC I. After the two projects were merged as shown in Figure 5.2. By comparing results to technical drawings a maximal mean deviation of 0.38 mm was found.

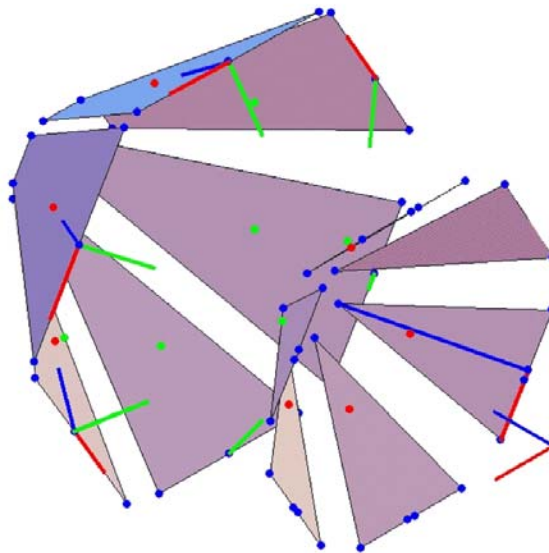


Figure 5.2 – Optical survey data (blue points) for MDC I and II. The local chamber coordinate systems are plotted in red-green-blue for the x y and z axes. The red points marking the physical centre points of the chambers on the aluminium frame, the green points the physical centres on the middle plane as used for the hits.

After the photometric procedure the relative positions of magnet structure and MDC II are known, and the positions of MDC I chambers respect to each other. But for the experiment MDC I was moved toward its nominal position, and its relative alignment respect to MDC II has to be calculated.

This was done measuring cosmic rays, which at sea level are mostly high energy muons. We used an opposite TOF/TOFINO sector trigger for taking cosmic with a mean data rate of about 80 Hz.

A sketch of reconstructed cosmic rays by inner chambers is shown in Figure 5.3, for the sector pair 1-4. The ray hits four chambers; we start from the optical survey alignment, and the position and orientation of MDC I is varied until the distances between measured points and projected ones in minimized for all the sector combinations. After the minimization procedure most of the sector residuals are around or below 100 μm .

The last part of the procedure consists on outer chambers alignment. For them no photometric measure was done in January 2004, so a procedure using straight tracks from no magnetic field runs was adopted.

Since we have an alignment of inner chambers, we can use straight tracks from these runs to align the outer chambers. The procedure consists on projecting the hits of inner chambers toward outer ones, and to minimize residuals of hit points by translating and rotating each outer chamber. Figure 5.4 shows a scheme of the used procedure.

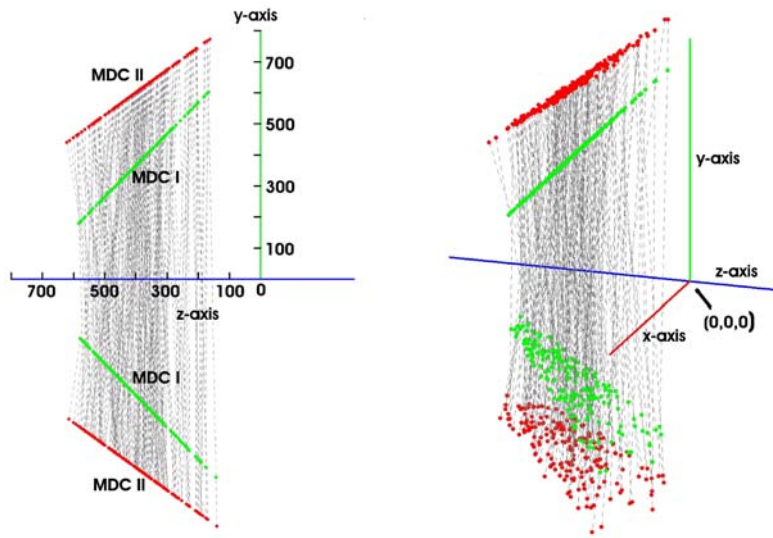


Figure 5.3 – Reconstructed cosmic rays with 4 hits in inner chambers (MDC I and II) for the sector combination 1-4. On the left a side view (the scale is in mm), on the right a more 3-D view.

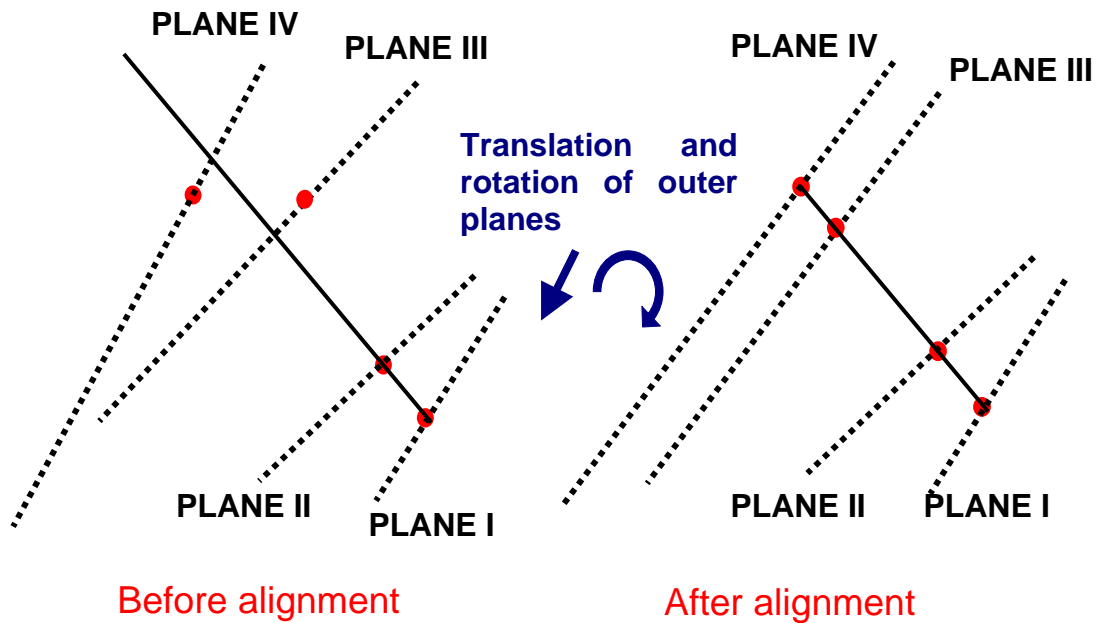


Figure 5.4 – Scheme of outer module alignment. The hit of the inner modules are projected towards outer chambers, and the distance between the projected hit point and the measured one is minimized.

The alignment obtained after all these steps can be checked by analysing elastic scattering, as it will be shown in the next paragraphs. In this case misalignment respect to different sectors and to the beam axis can be studied, and it is possible to estimate angular reconstruction.

5.3 Tracking algorithms

The momentum of a particle which crosses the spectrometer can be reconstructed by measuring its deflection before and after the magnetic field region.

For this purpose several tracking algorithms were developed and used. “Kickplane” is a low resolution algorithm which uses the information coming from the inner MDC modules and the META system, while “Spline” and “Runge-Kutta” perform high resolution momentum reconstruction using the full tracking setup.

In the following paragraphs a description of the tracking algorithms will be given.

5.3.1 Kickplane

By measuring the trajectory deflection of a charged particle inside a magnetic field region, it is possible to reconstruct its momentum value. Indeed a charged particle which crosses a magnetic field region undergoes to the Lorentz force, its kinetic energy remains unaltered but it feels a deviation from the original trajectory, in function of its momentum.

The trajectory in the region before the magnetic field is well determined by inner MDC chambers. But before the mounting of outer tracking system, and in particular for the November 2002 experimental run, the only information in the region after the magnetic field came from TOF and Shower hit positions. In order to reconstruct the track after the magnet another point in the space is needed.

The main idea for the momentum reconstruction with this setup is to use a virtual deviation plane, called “kick plane” [San00]. It consists on the assumption that the trajectory deflection in the field region happens abruptly in a well defined surface, called kick plane, in which the particle momentum undergoes to a transversal deviation P_T determined by the path integral of the track in the field, and not by the original momentum, as shown in Figure 5.5.

In this way the momentum P of a particle with charge Z can be calculated, on first approximation, by knowing the momentum kick P_T and the deviation angle $\Delta\theta$, by the formula:

$$\frac{P}{Z} = \frac{P_T(\theta, \phi)}{2 \sin\left(\frac{\Delta\theta}{2}\right)} \quad (\text{Eq. 5-6})$$

By projecting the track measured by inner MDC chambers towards kick plane we can determine the position upon this surface. From the kick plane position we can evaluate P_T , which is parameterised by knowing the magnetic field intensity in each point of the space (measured in the past by a special magnetic probe) and by simulation studies. From hit positions in TOF or Shower detectors we can calculate angular deviations, and at last momentum values.

For a better approximation the momentum deviation depends even on the particle path length inside the magnetic field region (as longer the particle stays inside the field, it undergoes to a higher deviation), which is proportional to the momentum kick $P_T = 2P \sin \frac{\Delta\theta}{2}$; to take into account to low momenta effects another parameter is needed.

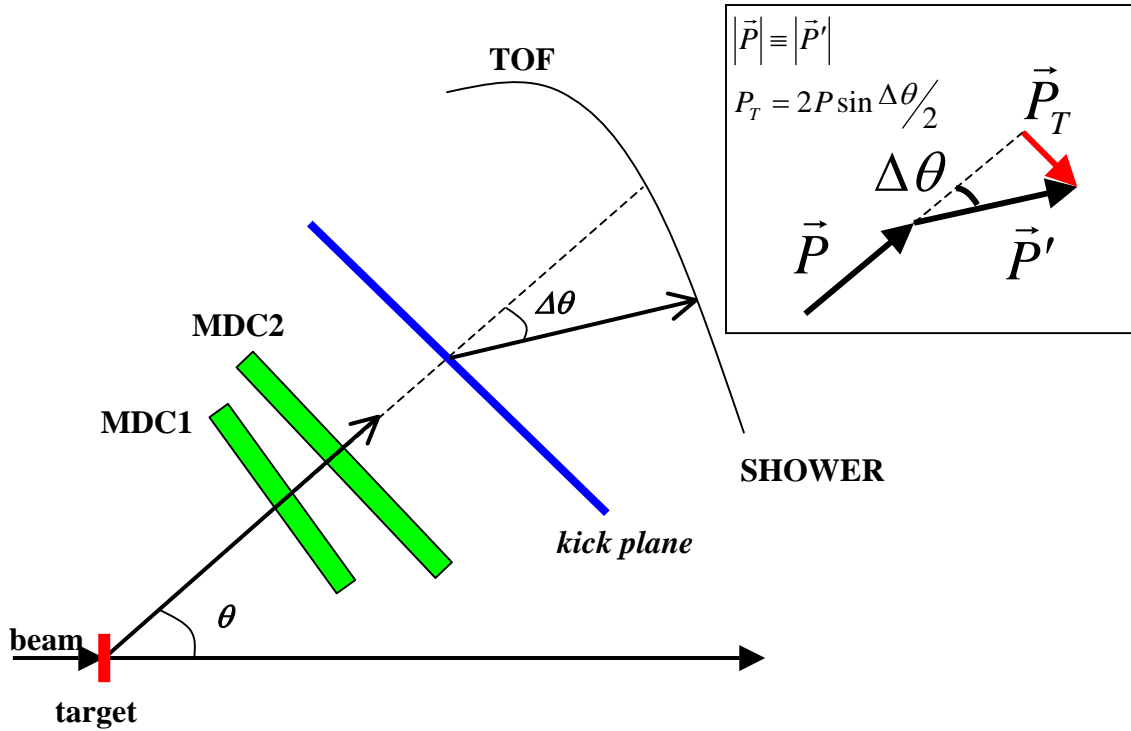


Figure 5.5 – Schematic view of the *kick plane* algorithm. It is based on the assumption that particle deviation in the magnetic field region happens abruptly in a well determined surface, called *kick plane*.

After these corrections, the correct the momentum formula will be :

$$\frac{P}{Z} = \frac{A(\theta, \phi)}{2 \sin\left(\frac{\Delta\theta}{2}\right)} + B(\theta, \phi) \cdot 2 \sin\left(\frac{\Delta\theta}{2}\right) + C(\theta, \phi) \quad (\text{Eq. 5-7})$$

The main limitation of this algorithm is that the track evaluation in the outer region depends on position resolution of META system, which is around 2-3 cm (much worse than the hundreds of microns of MDC chambers). The momentum resolution estimated in simulation for carbon reactions is about 10%, which is similar to the one DSL had.

For the proton experiment outer MDC setup was present and momentum reconstruction was performed by using different high-resolution methods. For this reason *kick plane* algorithm analysis will not be shown in this work.

Nevertheless the *kick plane* algorithm is still used for tracking in 3MDC sectors; for these sectors only one hit position after the magnetic field is not enough to determine the particle trajectory. An additional point is given by the hit projection into *kick plane* as in the low resolution case; by combining the information of the outer chamber and *kick plane* point is possible to evaluate the trajectory outside the field and after to recalculate momentum.

5.3.2 Spline tracking

The Spline algorithm is a high resolution tracking method which uses the hit positions in all the MDC chambers, and its trajectory reconstruction is based on interpolation by spline functions.

The equations of motion of a particle inside the magnetic field, considering (x, y, z) the coordinates in the laboratory system of the HADES experiment, are the following:

$$\frac{d^2 y}{dt^2} = \ddot{y} = \frac{1}{m} (\dot{z} B_x - \dot{x} B_z) \quad (\text{Eq. 5-8})$$

$$\frac{d^2 x}{dt^2} = \ddot{x} = \frac{1}{m} (\dot{y} B_y - \dot{z} B_y) \quad (\text{Eq. 5-9})$$

where B is the magnetic field and m is the mass of the particle.

If we use as momentum the expression:

$$P = m\dot{z} \sqrt{1 + \left(\frac{dx}{dz}\right)^2 + \left(\frac{dy}{dz}\right)^2} \quad (\text{Eq. 5-10})$$

we obtain, by combining the three previous expression, the differential equation:

$$\underbrace{\sqrt{1 + \left(\frac{dx}{dz}\right)^2 + \left(\frac{dy}{dz}\right)^2} \left(-B_z \frac{dx}{dz} - B_y \frac{dy}{dz} \frac{dx}{dz} + B_x \left[1 + \left(\frac{dy}{dz}\right)^2 \right] \right)}_{A(z)} = P \frac{d^2 y}{dz^2} \quad (\text{Eq. 5-11})$$

The Spline algorithm reconstructs particle trajectories by interpolating the hit points given by MDC chambers, two before the field and two after². It assumes a cubic spline model in the field region, while the trajectory outside the field is approximated by a quadratic function, as shown in Figure 5.6. The particle trajectory in the space is so determined by two spline fits, one for x and another for y coordinate.

After we have x and y in function of z , we can divide the trajectory in several steps (in general 50 steps are used) and calculate the left side of equation 5-11 point by point. By another cubic spline fit, we can evaluate this expression $A(z)$ and put it into equation 5-11, which becomes:

$$\frac{d^2 Y}{dz^2} = A(z) \quad (\text{Eq. 5-12})$$

² In sectors with only one MDC plane in the outer region, the algorithm evaluate the hit point in the kick plane surface and reconstruct a segment passing through this point and the MDC hit. By the intersection of this segment and the “virtual” plane of the missing chamber, the second point in the outer region is calculated.

By integrating two times the previous formula, we obtain the calculated value Y_i for each point in the trajectory. In this case $Y(z)/P$ will be a good representation of the track.

After we have calculated in this way the particle trajectory, we need to reconstruct its momentum. For this purpose we minimize the distance F (squared) between the calculated solution and what was obtained by the spline fit of the four MDC hit points:

$$F \equiv \left(\frac{Y_i}{P} + c_1 + c_2(z_i - z_0) - y_i \right)^2 \quad (\text{Eq. 5-13})$$

where c_1 and c_2 are the two integration constants.

At the end, by a least square fitting of the F quantity we can calculate the particle momentum P , as well as the two integration constants c_1 and c_2 , by simply imposing the derivative of F respect to the three constants is zero and by solving the linear equation system.

As shown here the Spline algorithm is based on approximations and interpolations of particle trajectories, so the momentum value it provides does not take into account fully the physical interaction of the particle inside the magnetic field. This means that this estimation can be improved, as it will be shown in the next paragraph. Nevertheless this algorithm has the advantage to be fast, because it does not require complicated or long calculations.

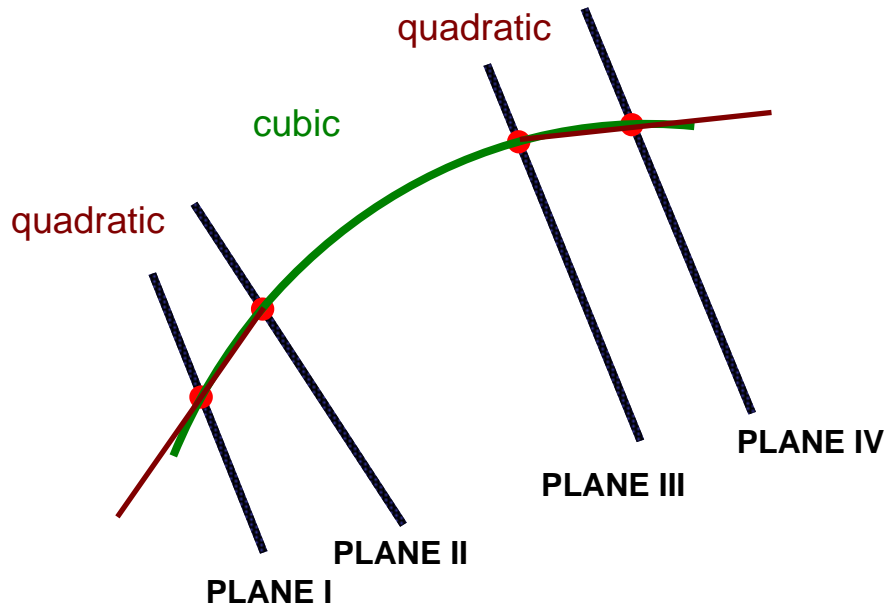


Figure 5.6 – The Spline algorithm: the trajectory of a particle is approximated by a cubic spline in the region inside the magnetic field, and by a quadratic spline in the outer region.

5.3.3 Runge-Kutta tracking

The Runge-Kutta algorithm is used to improve the high resolution tracking. By minimising the measured hit points and the fitted ones, it adjust the particle trajectory according to equation of motion, obtaining better values of momenta and angles.

A charged particle moving in a magnetic field has to satisfy the following equation of motion, which describes the action of Lorentz force on a moving charged particle:

$$\frac{d^2 \vec{x}}{ds^2} = \left(\frac{kq}{P} \right) \cdot \frac{d\vec{x}}{ds} \times \vec{B}(\vec{x}(s)) \quad (\text{Eq. 5-14})$$

where s is the path length, k is a constant which is proportional to the velocity of light, q is the charge of the particle in unit of e , P is the absolute value of the momentum and \vec{B} is the intensity of static magnetic field.

A track is then completely determined by five initial (boundary) values called track parameters, which in our case are direction angles (θ and ϕ), positions (r and z^3) and momenta. A track model is a set of cross positions in each detector surface for the track defined by certain track parameters. We will denote the track parameters as p and the track model as $f(p)$.

The track model can be formulated either as a full trajectory from an analytical or numerical solution of the equation of motion (5-14), or as a functional relation $f(p)$ which relates the impact points on specific chambers to some initial parameters p .

In the Runge-Kutta algorithm the track parameters p are estimated by minimizing the least square function:

$$Q(p) = (m - f(p))^T W (m - f(p)) \quad (\text{Eq. 5-15})$$

where m is the measurement vector, f is the track model (i.e. estimated hit vector from a given track parameter p), and W the weight matrix. The $Q(p)$ at minimum satisfies the χ^2 distributions.

In our simply case we assume the errors are uncorrelated respect to different track parameters, so W is of the form $W_{ij} = \delta_{ij} / \sigma_j^2$, where σ_j are the errors propagated by the track fitting.

In the presence of an inhomogeneous magnetic field, as the one of HADES spectrometer, an appropriate track tracing algorithm is needed to allow a particle to be travelled efficiently through a given detector setup. In our case it was used the fourth order Runge-Kutta method of Nystrom for this purpose [Pre02].

In order to minimize the ' χ^2 ansatz' $Q(p)$, we need a functional dependence of track interceptions on each detector surface for a given set of track parameter. In practice we need to differentiate Q with respect to the track parameter p and to find a zero value for the above equation:

³ In our case the track hit position is determined by the minimum approach distance between the track and the beam axis (r coordinate), and their minimum approach point projected into beam axis (z coordinate).

$$\frac{\partial Q}{\partial p} = -2(m - f(p))^T W \frac{\partial f}{\partial p} \equiv 0 \quad (\text{Eq. 5-16})$$

The partial derivative of $f(p)$ with respect to p can be computed by numerical differentiation:

$$\frac{\partial f_i}{\partial p_k} = \frac{f_i(p_0 + \Delta_k p) - f_i(p_0)}{\Delta p_k} \quad (\text{Eq. 5-17})$$

where $\Delta_k p = (0, \dots, \Delta p_k, \dots, 0)$. Consequently, the equation of motion has to be solved six times: one initial trajectory $f_i(p_0)$, five variational trajectories $f_i(p_0 + \Delta_k p)$.

We need an initial trajectory (zero trajectory) from where to start our computation; this track model is defined by the track parameters coming from MDC angles and positions, and Spline momentum. From these track parameters we evaluate the corresponding track model (trajectory) and calculate its intersection points with the MDC planes.

This information is put into equation 5-16. In order to solve it one applies Newton's method and obtains a recursive relation between the track parameters and the ones from the previous recursive step.

In a self consistent way new track parameter values are found with a χ^2 lower than in the previous step, and they are put newly into the equation .

When the χ^2 converges ($|q(p_i) - Q(p_{i-1})| < \varepsilon$, usually $\varepsilon < 0.001$ is enough), the fit procedure stops and give the final track parameters. So with Runge Kutta algorithm not only improves the momentum value but even the angular variables, as it will be shown in experimental data.

5.4 No Field runs

In the following paragraphs it will be shown the analysis on angular information of inner and outer MDC chambers, obtained in no field runs by means of elastic scattering channel.

In particular no field runs are the only ones where it is possible to study the behaviour of outer chambers, because in this case the outer polar angle information is not distorted by the bending of the magnetic field.

The elastic selection is performed by taking combinations of two fitted segments in the same event which hit opposite sectors, and belonging to the same kind of modules (so combining inner segments with only inner segment, outer segments with only outer segments). An additional condition was put at the 1st level trigger bit, selecting only event with multiplicity two in META and opposite sectors.

First the vertex reconstruction will be explored, which allows to estimate the position of the beam line. After, a study on azimuthal and polar angles will be shown.

5.4.1 Vertex reconstruction

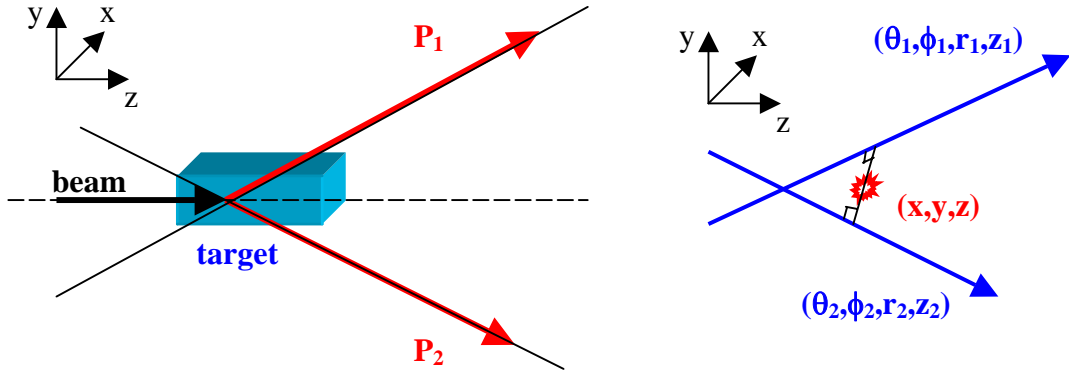


Figure 5.7 – Target reconstruction for a segment pair. The vertex is defined as the point of closest approach of the two straight lines.

One of the relevant information of a nuclear collision is where it took place. Assuming that the interaction between projectile and target is point like, we can define the interaction vertex as the point of closest approach of all primary tracks in the event.

By knowing the vertex position we are able to select only reactions which occurred inside the target region, we can check if there are other particle sources and where they are placed, and evaluate even the beam quality (Figure 5.7).

In our case we use fitted track segments belonging to opposite sectors, and we analyse separately inner and outer chambers. If we assume both the tracks are coming from the same interaction point, we can calculate the vertex point.

A line in the space is defined by four parameters, which in our case are the polar and azimuthal angles θ and ϕ , and the two position parameters r and z . Each pair of MDC chambers (inner and outer) reconstructs the trajectory of the particle which hit them, a straight line if we do not have magnetic field, and it provides the parameters which are needed to define geometrically the line.

Let's define a line in the space as:

$$\vec{P}_i = \vec{r}_i + \vec{\alpha}_i \cdot t \quad (\text{Eq. 5-18})$$

where \vec{r}_i is the position vector, $\vec{\alpha}_i$ is the direction vector and t is a free parameter.

The distance of a point \vec{x} from the line will be given by:

$$d_i = (\vec{r}_i - \vec{x}) \times \vec{\alpha}_i \quad (\text{Eq. 5-19})$$

We can then construct a χ^2 function as the squared sum of the distances between the vertex point and the two track lines:

$$\chi^2 = \sum_i \frac{d_i^2}{\sigma_i} = \sum_i \frac{((\vec{r}_i - \vec{x}) \times \vec{\alpha}_i)^2}{\sigma_i}$$

where σ_i is the position error given by the error propagation from MDC time fits.

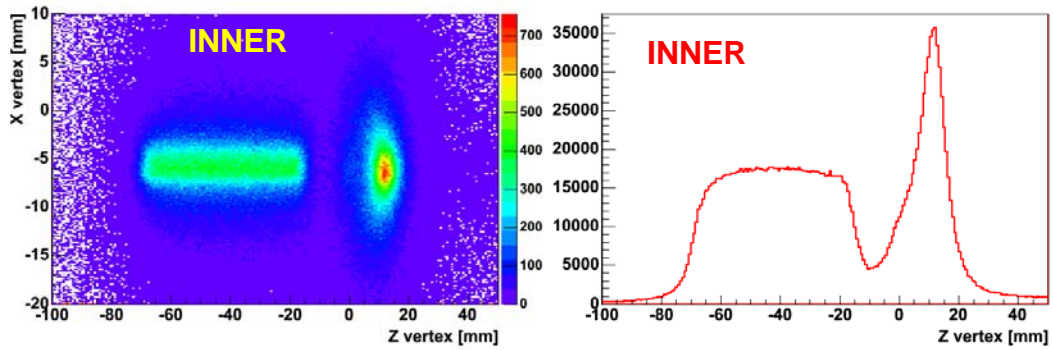


Figure 5.8 - Vertex reconstruction plots for inner MDC chambers. Left side: x vs z plot for vertex coordinates in the laboratory frame. Right side: z distribution. Apart from the target shape it is possible to see a prominent peak downstream, coming from the interaction of the beam with some material in the beam pipe.

The vertex position is so calculated by minimizing this χ^2 function, and the obtained χ^2 will be a measure of the minimum distance of the two tracks.

The left side of Figure 5.8 shows a two-dimensional plot of the reconstructed vertex (z vs x) for inner MDC chambers, in the laboratory coordinate system.

In the laboratory coordinate system the z axis corresponds to the beam line, greater values of z are in the downstream direction, while negative ones are upstream. The beam is so supposed to stay on $x=0, y=0$.

The target shape is correctly reconstructed and its 5 cm length is well visible, as shown in the right side of Figure 5.8, but it is possible to see a second structure at about 3 cm from the target in the downstream direction.

The reason of this second peak comes from the beam focusing in the early days of the January 2004 experiment, when the no field measure was done. Indeed if we check the x distribution we can see it is not centred to zero, but it has a displacement of about 6 mm; the beam direction was shifted respect to the centre of the beam pipe, and it hit a structure material placed downstream. In the field data, after the beam was better focused, this structure becomes negligible.

We want to select elastic pairs so we have to remove all the tracks coming from this second peak. This is done by selecting only pairs coming from the target region, applying a cut on the z vertex coordinate of $-80 \text{ mm} < z < -20 \text{ mm}$.

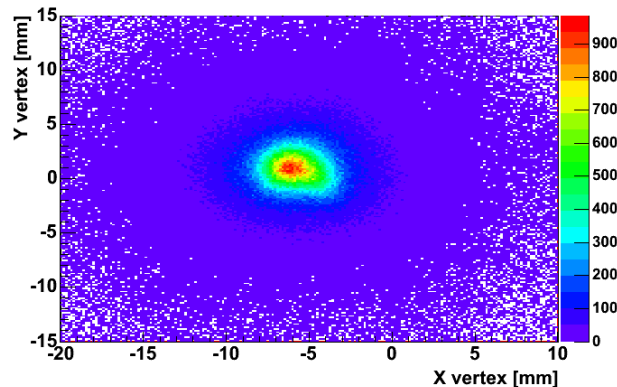


Figure 5.9 – Vertex plot for y vs x after the z selection ($-80 \text{ mm} < z < -10 \text{ mm}$). The estimated vertex reconstruction resolution is of about 2mm for both the coordinates.

Figure 5.9 shows the y vs x distribution after the z selection. By fitting in a range close to the peak the x and y one-dimensional distributions by a gaussian function, we obtain the position of the beam and its spread⁴ in x and y coordinates:

- $X_{\text{inner}} = -5.8 \pm 2.0$ mm
- $Y_{\text{inner}} = 0.8 \pm 1.9$ mm

The same procedure can be repeated even for the outer MDC chambers.

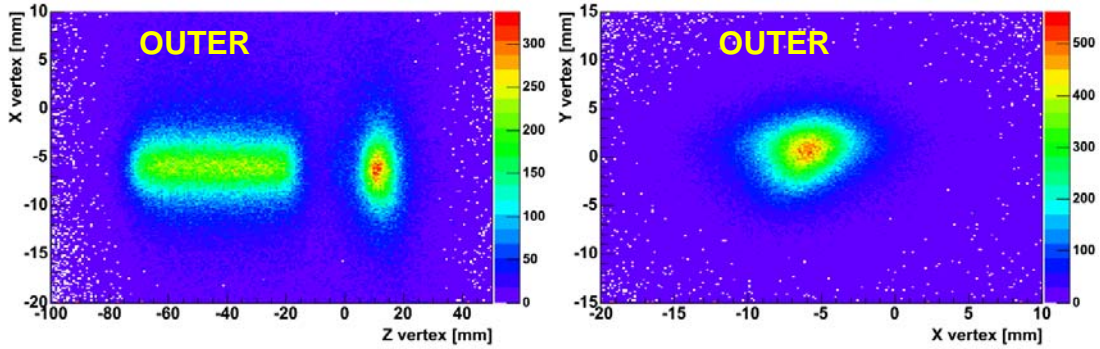


Figure 5.10 – Vertex plots for outer MDC chambers (left side: x vs z - right side: y vs x after the -80 mm $< z < -10$ mm selection). We can see x and y widths are larger respect to inner module ones, because of their larger distance from the target region, and so their less effective reconstruction power.

The vertex plots for outer MDC chambers are shown in Figure 5.10. Even for outer chamber pairs the second peak is prominent, so the same z selection was applied.

We can see that the x and y distributions are broader respect to the inner chamber ones, as it is shown by the results of gaussian fits near the peak:

- $X_{\text{outer}} = -6.0 \pm 2.4$ mm
- $Y_{\text{outer}} = 0.6 \pm 2.5$ mm

This is connected to the fact that outer chambers are farther from the target region, so the error on hit position propagated toward the target region becomes larger respect to the inner ones.

As we can see, the centres of vertex positions are consistent with what evaluated by the inner modules.

5.4.2 Azimuthal angle

After we have selected track pairs coming from the target region, so after removing the second peak, we can evaluate angles by using elastic pairs.

The first considerations come from azimuthal angles. Coplanarity of the two elastic protons is expressed by the equation:

⁴ The sigma of the gaussian fit is the quadratic sum of the beam width plus the vertex reconstruction resolution. Considering that the MDC chambers have a position resolution of ~ 100 μm , the corresponding vertex precision can be considered as negligible.

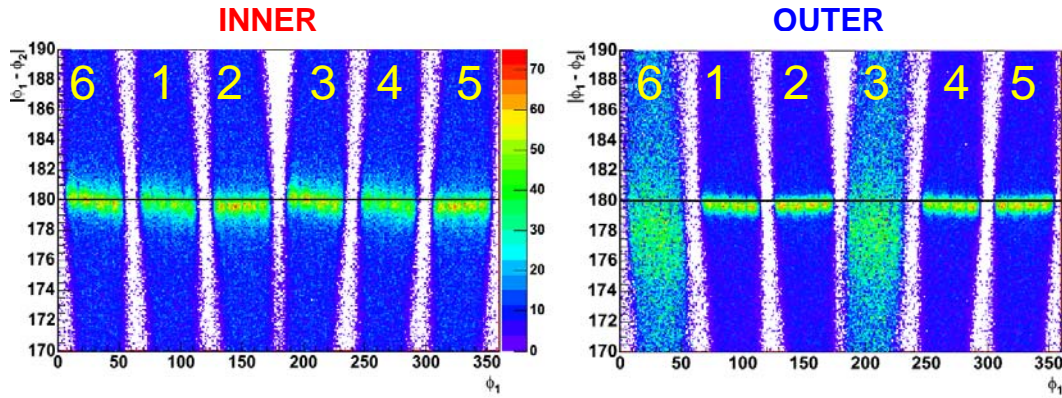


Figure 5.11 – Difference in azimuthal angles between two tracks hitting opposite sectors, for inner chambers (left side) and outer chambers (right side). For outer chambers the counts on 3MDC sectors are multiplied by a normalization factor in order to compare their distributions to other sectors onew.

$$|\phi_1 - \phi_2| = 180^\circ \quad (\text{Eq. 5-1})$$

so we can plot this difference to check the azimuthal angle resolution of the alignment.

Figure 5.11 shows the difference in azimuthal angle of opposite sector pairs in function of the azimuthal angle ϕ of one of the two tracks, separately for inner (left plot) and outer (right plot) segments.

In the laboratory notation, the first sector is placed between 60° and 120° , the second one between 120° and 180° and so one, while the sixth stays between 0° and 60° . In the right plot we can see the lose in angular resolution for 3MDC sectors (the 3rd and the 6th sectors), where there was present only one outer module and so for the angular reconstruction the lower resolution kickplane information was used.

Even if no particle identification was performed, by simply using tracks in opposite sectors we are able to find the elastic one. Indeed the peak at 180° is well defined and prominent, apart from 3MDC modules.

By comparing inner and outer chambers (only 4MDC sectors), the outer ones have a better resolution respect to the inner, the contrary respect what was shown in paragraph 5.4.1 for the position information by vertex reconstruction. This means that the particle direction is better reconstructed by outer planes, even because it is calculated on a longer distance so spreads are reduced respect to inner chambers. By checking the behaviour of the 180° peak in function of the azimuthal angle, some small systematic deviation are present, for some sectors the distribution seems a bit tilted, instead to be a perfect horizontal line. The alignment procedure worked quite well, but some improvements can be done.

The main reason of the small systematic deviations is the beam position not centred along the z axis but a bit shifted, as shown in Figure 5.9 and Figure 5.10; this fact introduces a low order effect on the direction reconstruction in laboratory coordinate system. Moreover at the moment the hypothesis of a tilted beam direction respect to z axis is under study, and it can explain systematic deviations and larger resolution values than expected⁵.

⁵ The alignment procedure calculates absolute positions in the laboratory coordinate system. But an eventual deflection of the beam alters the reconstructed angular variables, and also momenta.

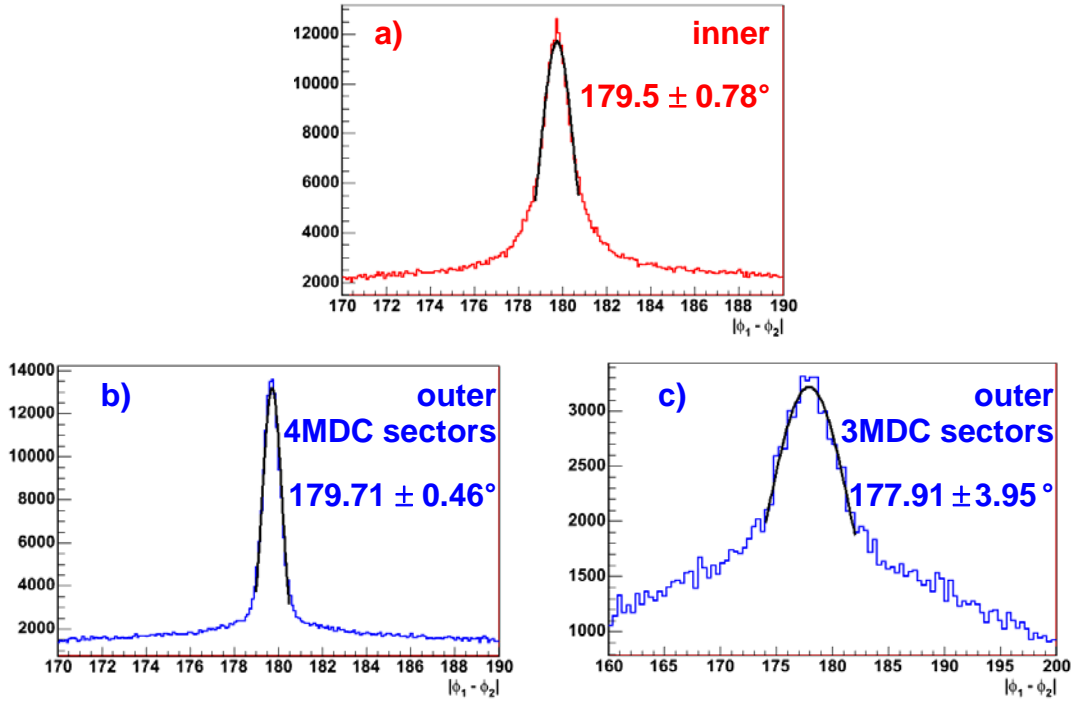


Figure 5.12 – Coplanarity plots for different chambers: a) inner MDC modules; b) outer MDC modules, 4MDC sectors; c) outer MDC modules, 3MDC sectors. The gaussian fit near the peak provides an estimation of the single segment azimuthal angle resolution.

Looking to outer chambers - 3MDC sectors, the bump width is much broader and not centred in the correct 180° position. This is due to the poor resolution of one chamber segment reconstruction, which does not allow to obtain high resolution tracking and alignment.

The plots of Figure 5.12 show differences in ϕ for inner and outer segments, in the latter separately for 4MDC and 3MDC sectors.

Assuming the azimuthal resolution is the same for both the opposite sectors chambers ($\sigma_{\phi_1} \equiv \sigma_{\phi_2}$), we can evaluate the average single chamber ϕ resolution by the relation:

$$\sigma_{|\phi_1 - \phi_2|} = \sqrt{\sigma_{\phi_1}^2 + \sigma_{\phi_2}^2} \equiv \sqrt{2}\sigma_{\phi} \quad (\text{Eq. 5-20})$$

If we divide by $\sqrt{2}$ the fit widths shown in Figure 5.12, we obtain the following resolution values:

$$\sigma_{\phi}^{inner} = 0.6^\circ$$

$$\sigma_{\phi}^{outer 4MDC} = 0.3^\circ$$

$$\sigma_{\phi}^{outer 3MDC} = 2.8^\circ$$

5.4.3 Polar angle

An analysis similar to what was done for the azimuthal angle ϕ can be applied even for the polar angle θ . In this case the useful relation is:

$$\tan \theta_1 \cdot \tan \theta_2 = \frac{1}{\gamma_{CM}^2} \quad (\text{Eq. 5-2})$$

where for 2 GeV collisions (no field run) $1/\gamma_{CM}^2 = 0.4841$.

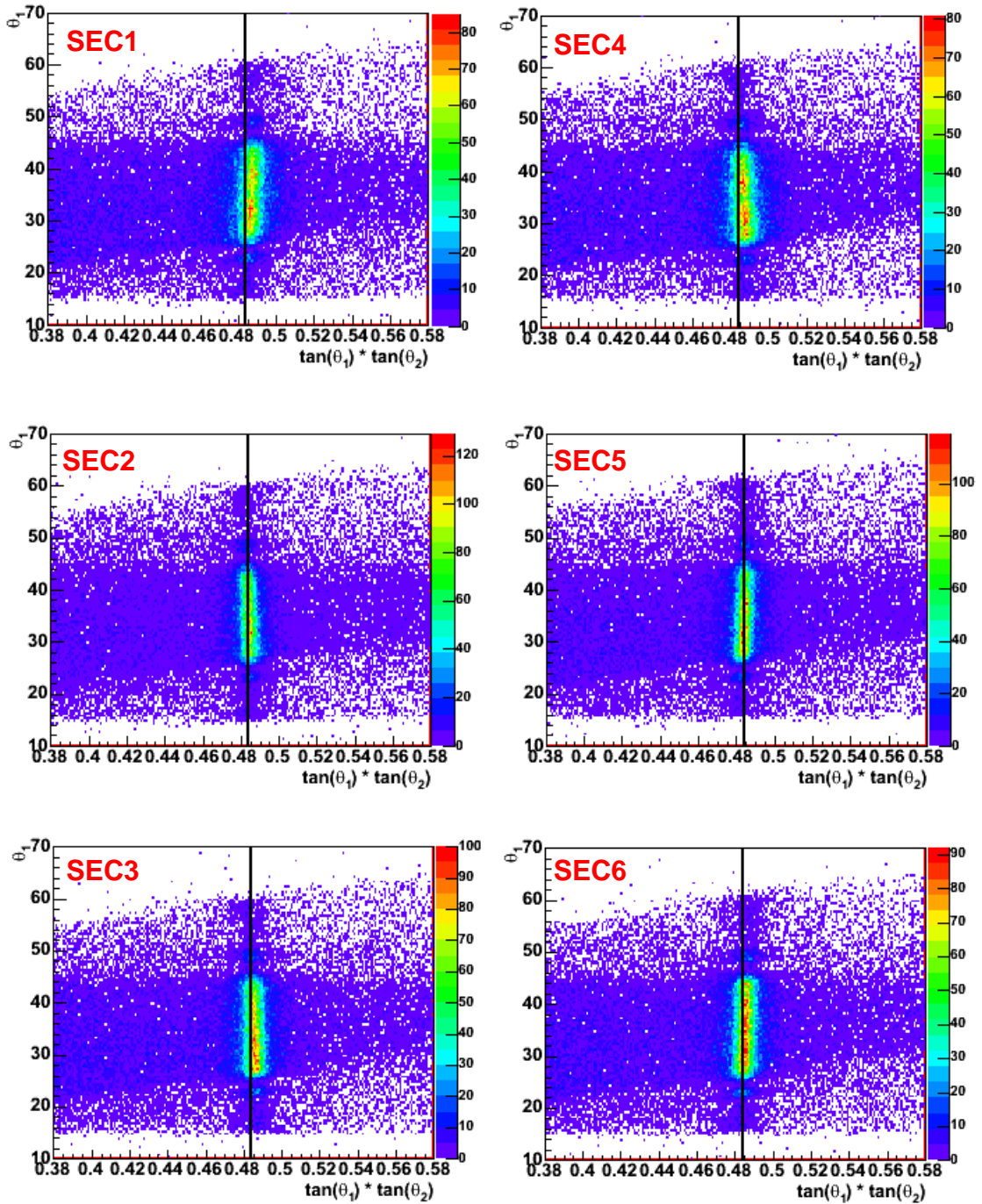


Figure 5.13 – 2D plots for θ_1 vs $\tan\theta_1 \cdot \tan\theta_2$ inner chambers, sector by sector; the black line represents the prevision value obtained by the reaction kinematics. The chambers show a quite good alignment, and no systematic deviations are present.

Figure 5.13 and Figure 5.14 show sectorwise distributions for θ_1 vs $\tan\theta_1 \cdot \tan\theta_2$, respectively for inner and outer modules.

The plots are very useful in order to establish the quality of the alignment, because they are strongly dependent on the alignment.

In the outer chambers we can see the not good resolution of 3MDC sectors, but even with this configuration the peak is visible and close to the kinematical prediction.

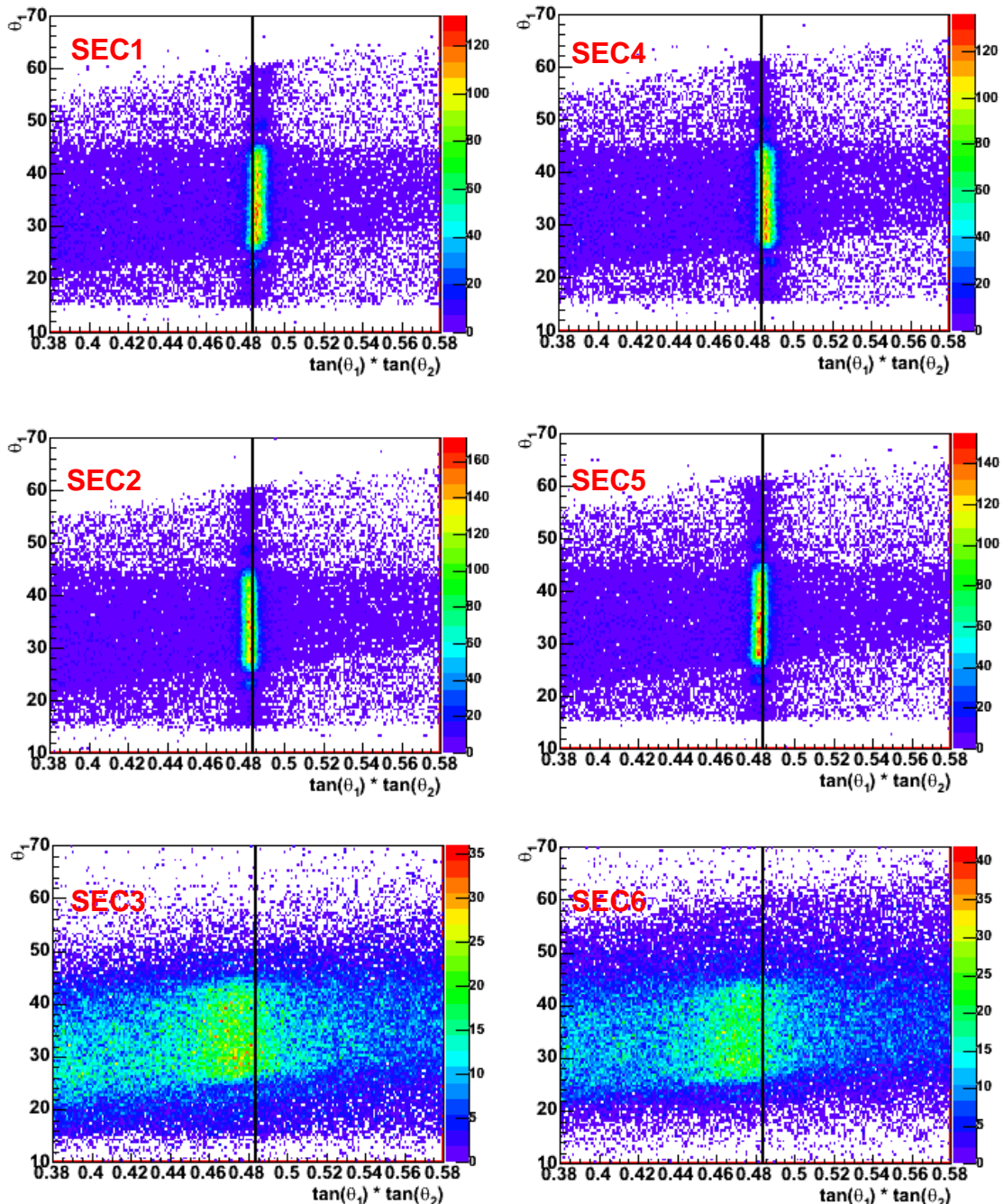


Figure 5.14 - θ_1 vs $\tan\theta_1 \cdot \tan\theta_2$ plots for outer chambers, sector by sector; the black line is the kinematical prediction. Even these chambers show a good alignment, apart for 3MDC sectors.

In Figure 5.15 there are the $\tan\theta_1 \cdot \tan\theta_2$ plots for different chambers. The peaks were fitted by gaussian functions, and the obtained centroids stay in the position expected by theoretical calculation. Even in this case we can see that 3MDC sectors geometry needs an improvement, but a part from this consideration the numbers show the high quality of the alignment obtained by the described procedure.

At the moment new alignment procedure are under study, which could achieve even better results. In particular it is under study how to use the additional information coming from proton-proton elastic scattering. But no one of these procedure was yet tested in January 2004 data.

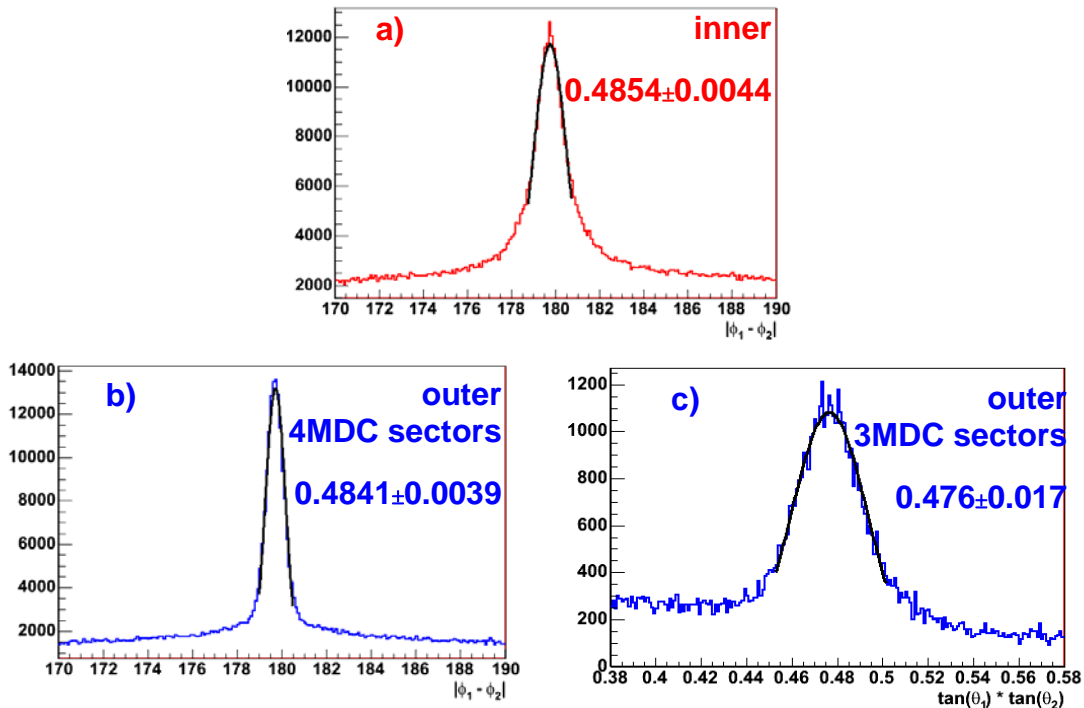


Figure 5.15 - $\tan(\theta_1) \cdot \tan(\theta_2)$ distributions for different chambers: a) inner MDC modules; b) outer MDC modules, 4MDC sectors; c) outer MDC modules, 3MDC sectors. The peaks were fitted by gaussian functions, and the fit values are reported in the plots.

5.5 Field data – Spline Tracking

While the no field data were used only for calibration and alignment purposes, the most of data were acquired with magnetic field, in order to use deflection to reconstruct particle momenta.

But in between the to magnet setup the beam focusing was changed and improved, and it has to be rechecked; the same alignment analysis has to be redone, in order to see eventual effects of the magnetic field on angular resolution.

Because of the magnetic deflection, for alignment purposes the information from outer segment cannot be used, so it will be shown the analysis only for the inner one.

Momentum reconstruction will be studied and resolution will be evaluated, by using spline tracking algorithm.

The analysis of Runge Kutta algorithm and the comparison with spline will be shown in the paragraph 5.6.

5.5.1 Vertex reconstruction

The same procedure of paragraph 5.4.1 was applied for field data.

This time we do not use the segment information from MDCs, but we use the full tracks reconstructed by spline algorithm. A full track is made by the correlation of inner segment, outer segment and META hit, and it carries with itself the information of the reconstructed momentum.

In Spline case angular and position parameters are given by the inner MDC segment. All the plot that will be shown were made using these variables.

But this time we can use an additional information, which was not present in the files without magnetic field, while trying to select our proton elastic pair. By the trajectory deviation inside the magnetic field the tracking algorithm evaluate the charge polarity of the particle; so we can select positive charged particles hitting opposite sectors, to select our protons.

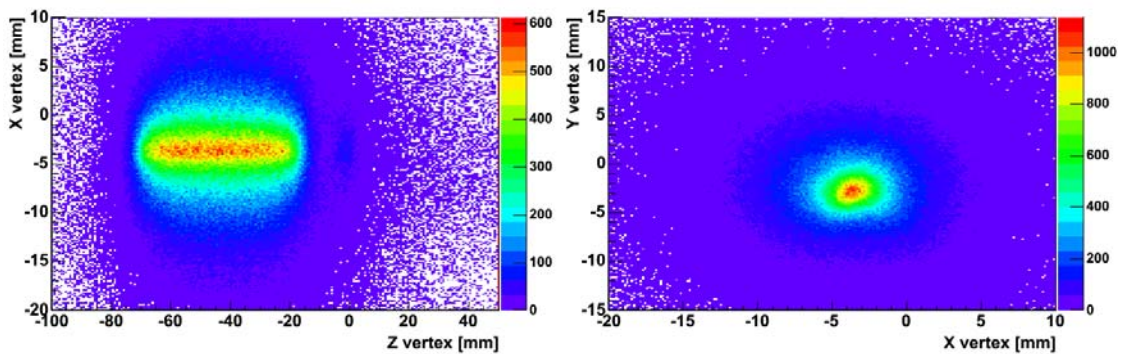


Figure 5.16 - Vertex plots for opposite sector tracks (left side: x vs z - right side: y vs x). With the new beam focusing, the second peak now is negligible and the cut on z is not needed anymore.

Figure 5.16 shows vertex plots for field data, after the beam focusing. As it is shown in the y vs x plot (left side), the beam spot was shifted of few millimetres, in both x and y directions; in particular it results better centred in the x position. The main result of this improved focusing is that now the second peak (left plot) is reduced respect to no field runs, because the number of particles which hit the material was strongly reduced.

In this case we can see the selection on z vertex coordinate is not needed anymore, because this contribution became negligible.

One dimensional distributions for x and y were filled and fitted by a gaussian function. The results are:

- $X_{\text{spline}} = -3.6 \pm 2.5$ mm
- $Y_{\text{spline}} = -2.7 \pm 2.5$ mm

The widths are broader respect to what obtained in no field data, but we have to consider that a fraction of the field is still present in MDC chambers, in particular for those plane closer to the coil. This low field influences the track reconstruction, and can produces a decrease in the resolution.

5.5.2 Azimuthal angle

The same analysis of 5.4.2 was performed for field data.

Figure 5.17 shows coplanarity distributions in function of the azimuthal angle for one particle of the pair (left side). We can see the distribution is well centred at 180° as expected, and no strong systematic behaviour can be seen from the plot.

Indeed we can see the worsening of the resolution does not allow to do a fine check of the alignment.

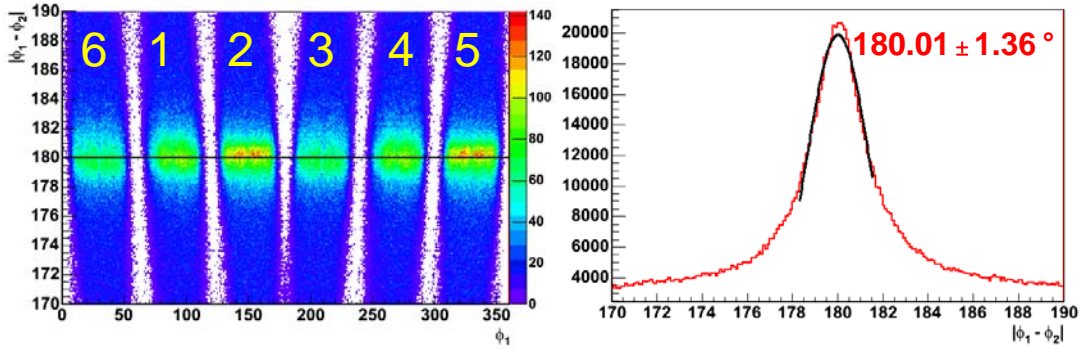


Figure 5.17 – Azimuthal plots for Spline tracking. On the right side ϕ_1 vs $|\phi_1 - \phi_2|$, on the left one single $|\phi_1 - \phi_2|$ distribution and the results of a gaussian fit.

Checking the one dimensional spectrum of the right plot, the main peak is closer to 180° than before (mainly due to the beam closer to z axis), but the width of the gaussian fit is about the double of what was evaluated before. We can compute the angular resolution as before, obtaining a value of $\sigma_\phi = 0.96^\circ$ (in no field data it was 0.6° for inner MDC chambers).

5.5.3 Polar angle

In field data the kinetic energy of the projectile proton was 2.2 GeV, so the polar angle kinematical value is $1/\gamma_{CM}^2 = 0.4598$.

Figure 5.18 show the one dimensional distribution for $\tan\theta_1 \cdot \tan\theta_2$, averaged all over the sectors. We can see the peak is in the correct position. A gaussian fit was done and the width shows even in this case a worsening, consistent with what was found for azimuthal angles.

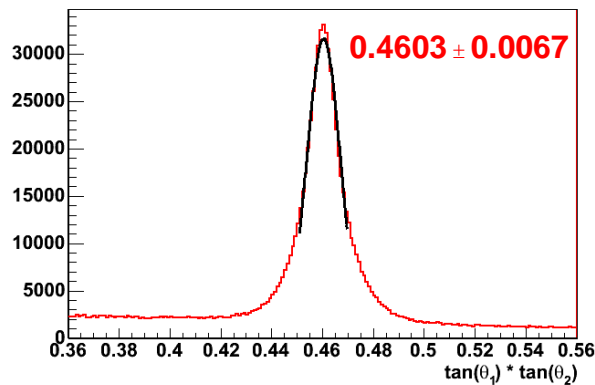


Figure 5.18 – Distribution for $\tan\theta_1 \cdot \tan\theta_2$ integrated for all the sectors.

In Figure 5.19 θ_1 vs $\tan\theta_1 \cdot \tan\theta_2$ plots are shown sector by sector. The distributions are well centred to the kinematical value, but some systematic deviations from the vertical line are visible, in particular in the low polar angle regions. Nevertheless the achieved alignment is quite good and it can be used in field data, giving good results.

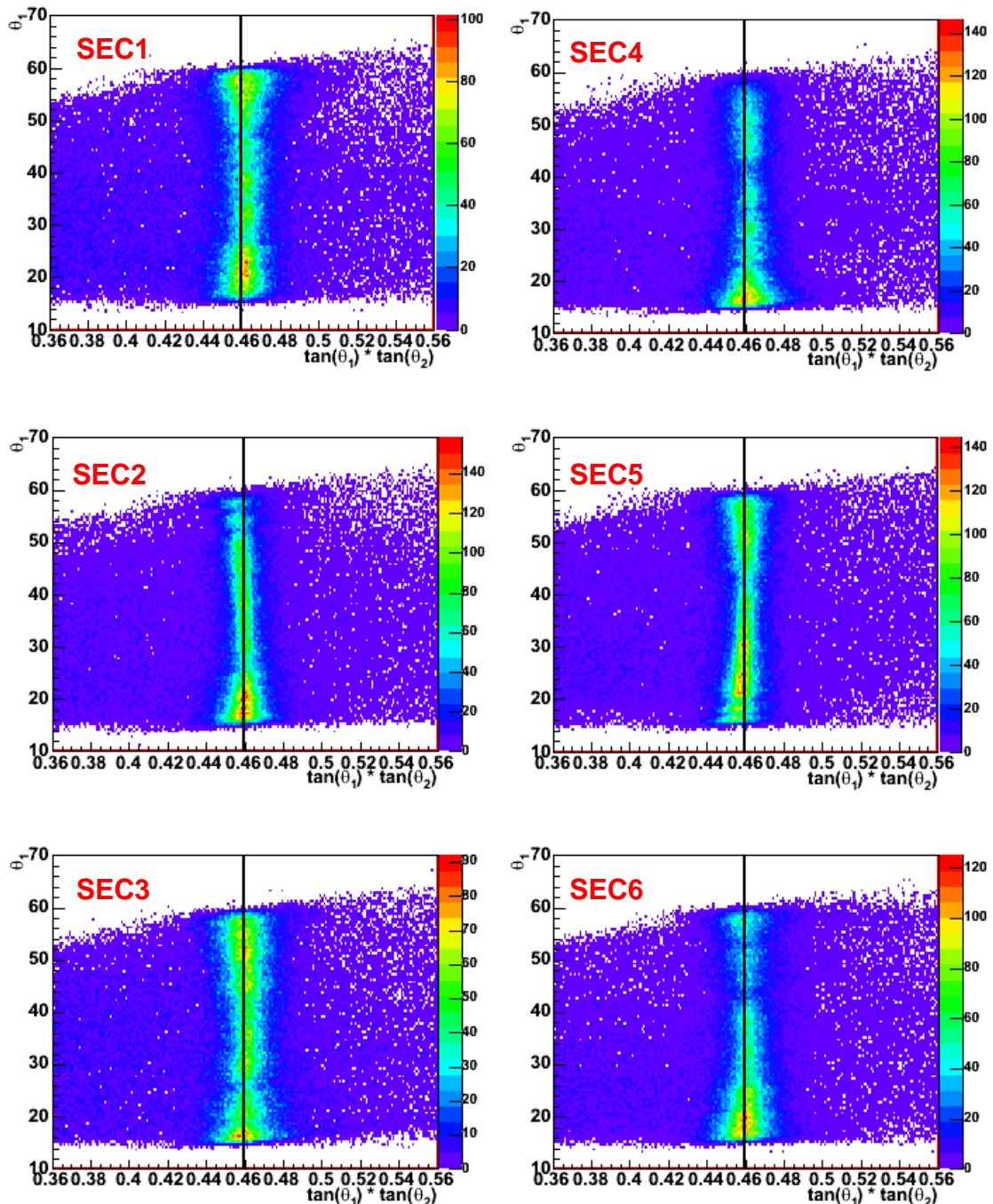


Figure 5.19 - 2D plots for θ_1 vs $\tan\theta_1 \cdot \tan\theta_2$ for positive charged spline tracks, sector by sector; the black line represent the kinematical value. The distributions are well centred to the expected position. Nevertheless some small deviations are still visible.

5.5.4 Elastic selection

By combining the angular information about polar and azimuthal angles we can choose pairs close to the expected peak positions, in order to select only elastic pairs and take out most of the background.

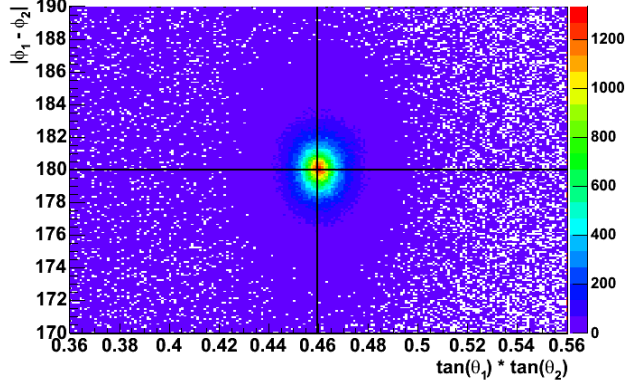


Figure 5.20 - $|\phi_1 - \phi_2|$ vs $\tan\theta_1 \cdot \tan\theta_2$ plot. Elastic pairs are placed in the region of the main peak. The black lines show the kinematical prediction

In Figure 5.20 we can see how the use of topology can identify pairs belonging to elastic scattering.

First of all we can define two variables given by:

$$\Phi \equiv |\phi_1 - \phi_2|, \quad \Theta \equiv \tan \theta_1 \cdot \tan \theta_2 \quad (\text{Eq. 5-21})$$

So we can construct a χ^2 function as:

$$\chi^2 = \frac{(\Phi - \Phi_0)^2}{\sigma_\Phi^2} + \frac{(\Theta - \Theta_0)^2}{\sigma_\Theta^2} \quad (\text{Eq. 5-22})$$

where Φ_0 and σ_Φ are centroid and sigma of the gaussian fit over azimuthal difference distributions (Figure 5.17), while Θ_0 and σ_Θ are the fit results obtained by the product of polar angle tangents. In this case elastic pairs should stay at the peak positions, so their χ^2 value should be minimal.

On the left plot of Figure 5.21 the χ distribution is shown. The main peak corresponds to elastic pair so we can select them by introducing an upper cut, in order to strongly decrease the background coming from other processes (which is almost constant). A selection on pairs with $\chi < 3$ was applied, in order to have most of the elastic pairs with the lower background contamination. The right plot of Figure 5.21 shows how the cut selected pairs along the main peak (the black dots correspond to rejected pairs by the cut).

By applying the topologic angular selection for positive charged pairs, we are able to select elastic pairs and to evaluate their momentum reconstruction.

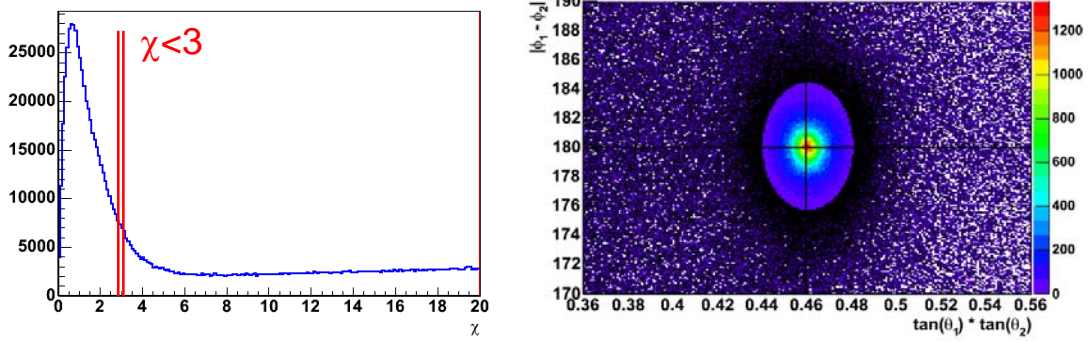


Figure 5.21 – χ distribution for positive charged pairs (left side). By using a cut on $\chi < 3$ it is possible to separate elastic pairs from the background. On right side the elastic topologic spectrum is shown after this cut; the black dots correspond to rejected pairs.

5.5.5 Momentum reconstruction

Assuming that a tracks is a proton coming from an elastic reaction, from the polar angle θ it is possible to calculate the “theoretical” value of momentum, and to compare it with the results of the tracking algorithm.

Indeed the relation that correlates momenta to polar angles (for elastic scattering) is given by the formula:

$$p(\theta) = \frac{p_{proj}}{\cos \theta + \gamma_{CM}^2 \sin \theta \cos \theta} \quad (\text{Eq. 5-3})$$

where p_{proj} is the momentum of the incoming proton (projectile).

After we have selected elastic pairs from spline tracking, by the χ cut, we can plot the ratio between kinematical prediction $p(\theta)$ and spline value of momentum p belonging to one of the two protons, as shown in Figure 5.22. All the distributions are not normalized, but come simply from the values obtained by the tracking (no multiplication factors).

We can see all the peaks are centred to value “one” even for 3MDC sectors, showing that the momentum provided by the algorithm works well, and so the alignment is correct. We can do a gaussian fit⁶ over the peak, in order to estimate the momentum resolution of the algorithm.

The obtained momentum resolution values depend even on the polar angle resolution, which is used to estimate the theoretical value.

Four MDC sectors present a resolution close to 5%, apart from the 1st sector which shows a broader distribution connected to the switched off wire layers on inner planes (less points for time fitting, and so worse resolution).

About three MDC sectors, sector 3 have a bad resolution (16%) respect to the others, but for this sector we have to remember only one MDC chamber was used for the reconstruction of the outer segment, and it had only four wire layers working. In this case the time fit was not possible (we need at least 5 points to fit a line in the space), so the resolution is what comes from the cell size. The other sector presents a resolution (7.5%) which is even better than the 1st sector, and below the 10% expected

⁶ In reality the momentum p does not follow a gaussian distribution, while the quantity $1/p$ presents this shape, because of the particular geometry of the HADES magnetic field. But we are interested in momentum resolution, so the fit was done over momentum.

from the low resolution kickplane algorithm. This tells us the spline reconstruction works quite well even in 3MDC sectors.

In order to see if there are systematic deviations we can see resolution plots in function of the polar angle, as shown in Figure 5.23.

It is well evident that at low polar angles, which correspond to higher momentum values, a systematic deviation is present in more or less all the sectors. This effect is connected to position chamber in the laboratory frame after alignment, which is close to the real value but it still needs a second order improvement.

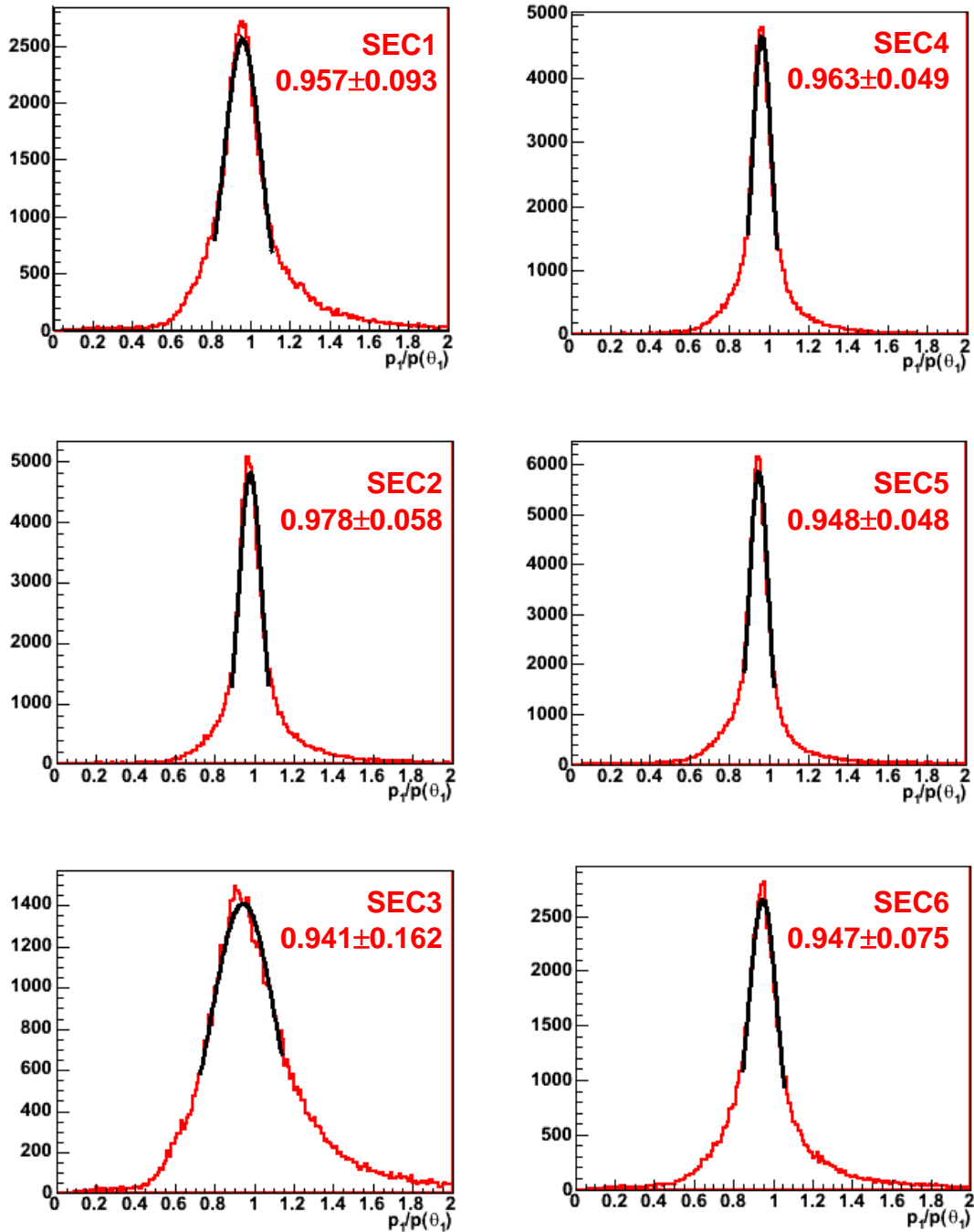


Figure 5.22 – Ratios between reconstructed momentum from spline and kinematical prediction, by using the polar angle θ . The reported values are the results of a gaussian fit in the peak region.

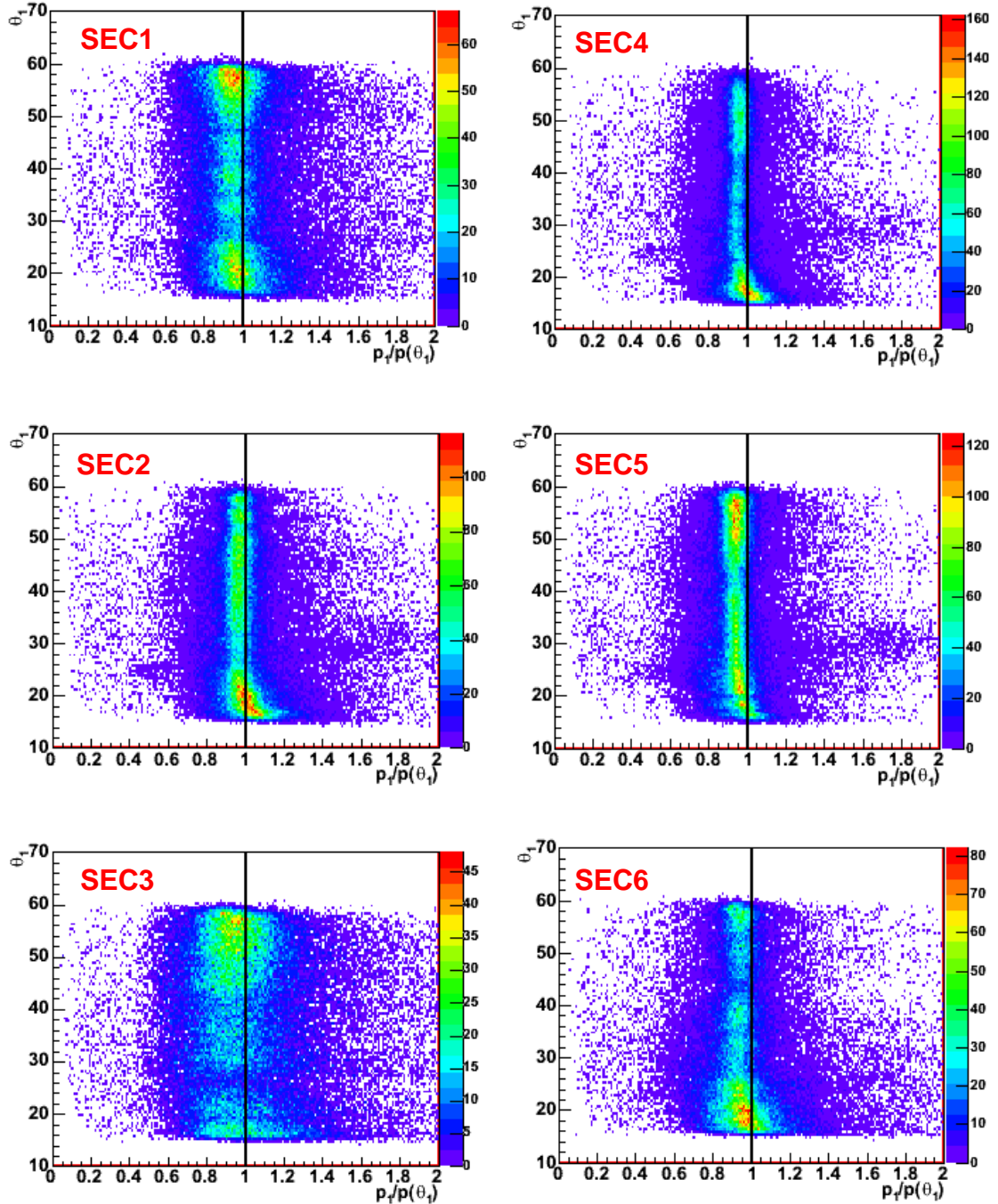


Figure 5.23 – Ratios between kinematical and reconstructed momentum for spline tracking, in function of polar angles.

Figure 5.24 shows momentum times polar angle (left), and the momentum of the first proton versus momentum of the second one (right), for the sector pair which showed better resolution (sectors #2 and #5).

We can see how momenta and polar angles are correlated, and how in the lower angle region the spread in momentum becomes larger, due to high momentum values which are difficult to reconstruct because of their small deviations. The HADES acceptance for elastic pairs is well visible in these plots.

We have to consider in resolution evaluation that the minimum value of proton momenta is of about 800 MeV/c, while in general HADES is best suited to detect

leptons which possess lower momenta. So we can consider these values as a sort of upper limit to the actual momentum resolution for leptons.

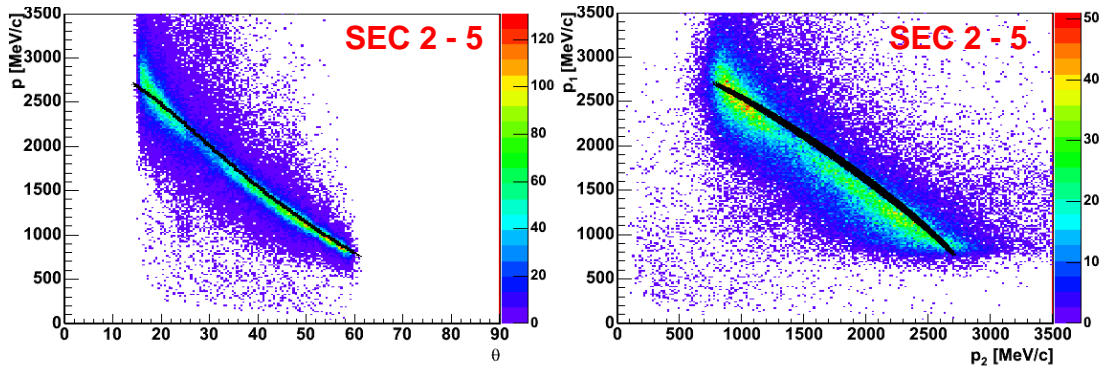


Figure 5.24 - Plots for sector pair 1-4, which shows a better resolution. Momentum versus polar angle (right side), and momentum of a proton respect to the momentum of the other one. The black lines represent theoretical predictions.

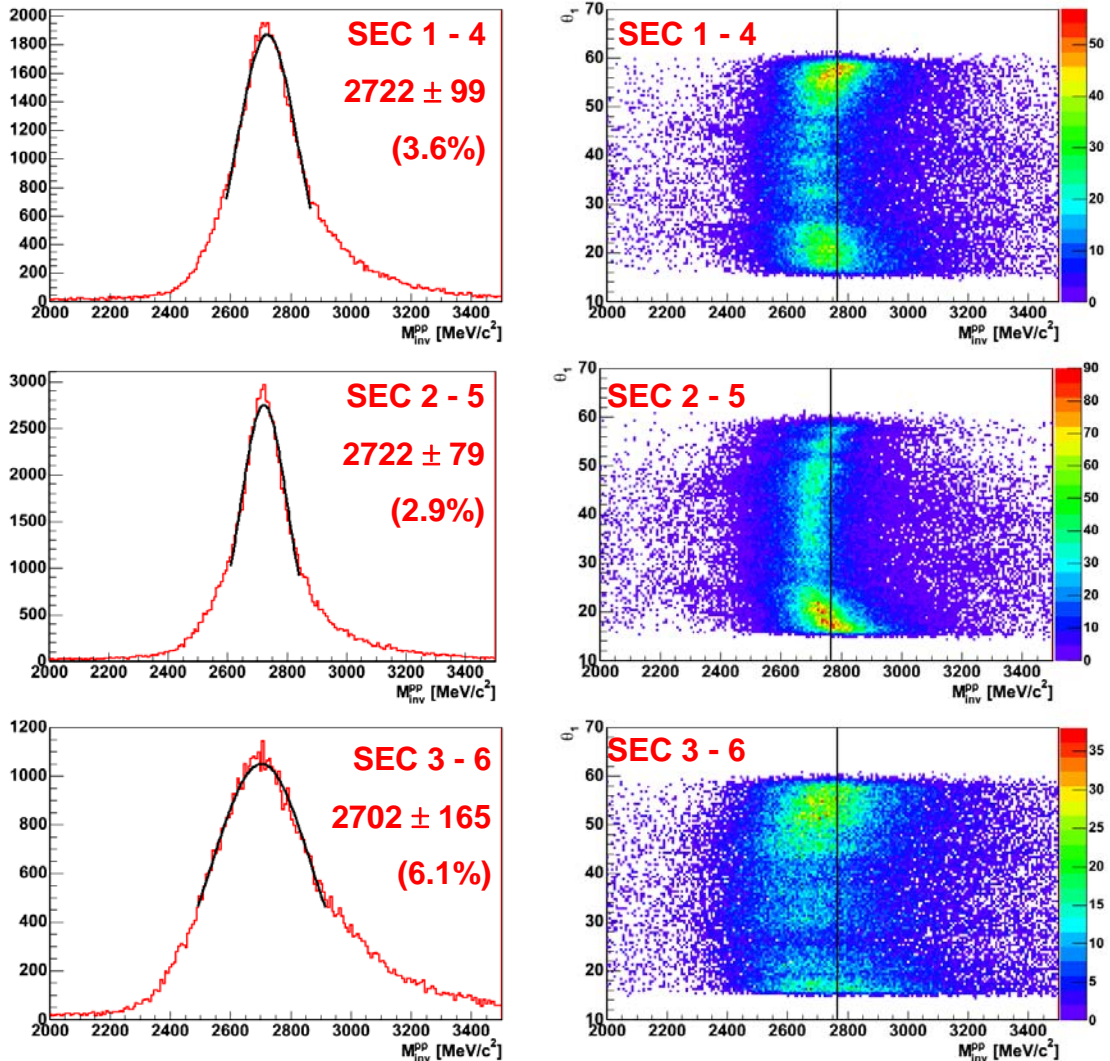


Figure 5.25 – Missing mass distributions on the left, and in function of polar angle of one proton on the right, for different sector pairs. The kinematical value of proton-proton invariant mass is $2768 \text{ MeV}/c^2$, and it is indicated by the black lines.

Indeed we are interested in evaluation of invariant mass resolution, instead of single proton one. Knowing the proton momentum vector \vec{p}_1 , from the measured momentum and polar angles values, we can calculate the total energy E_i and so the value of the pair invariant mass:

$$M = \sqrt{(E_1 + E_2)^2 - (\vec{p}_1 + \vec{p}_2)^2} \quad (\text{Eq. 5-5})$$

In Figure 5.25 invariant mass distributions are presented for different sector pairs. The peaks are at the nominal position, while the best resolution value we can obtain is 2.9% in sector pair 2 and 5. The plots in function of polar angles show the same systematic behaviour of single track resolution plots.

Indeed in the “central” region of polar angles (around 40° , which corresponds to a momentum value of ~ 1500 MeV/c), the obtained invariant mass is underestimated respect to the kinematical value. Something similar is present even in the right plot Figure 5.24: there is an agreement at the edges of acceptance, while in the central region the experimental values seem lower.

The spline algorithm calculates momentum by interpolation, so it does not take into account the physics of the particle interaction with the magnetic field. Its momentum reconstruction will be improved by the Runge Kutta tracking.

5.6 Field Data – Runge Kutta Tracking

Runge Kutta algorithm takes position and angular variables from the inner MDC segment, momentum values from the spline algorithm, and it does a kinematical refit of the tracks, providing a new set of parameters (θ , ϕ , r , z and p). The quality of these new values, different from the ones used by Spline tracking, will be studied in the next paragraphs and their improvement will be estimated respect to previous values.

5.6.1 Vertex reconstruction

Figure 5.26 shows vertex plots for Runge Kutta algorithm, by using polar angles and hit positions recalculated by the tracking code.

In order to understand the differences respect to values obtained by the segment, Figure 5.27 shows comparison of one dimensional distributions for vertex coordinates between old and new values.

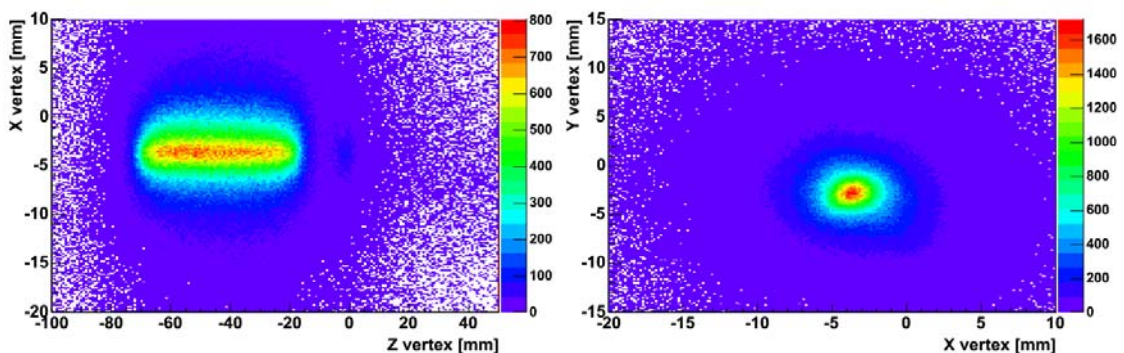


Figure 5.26 – Vertex plots for Runge Kutta algorithm.

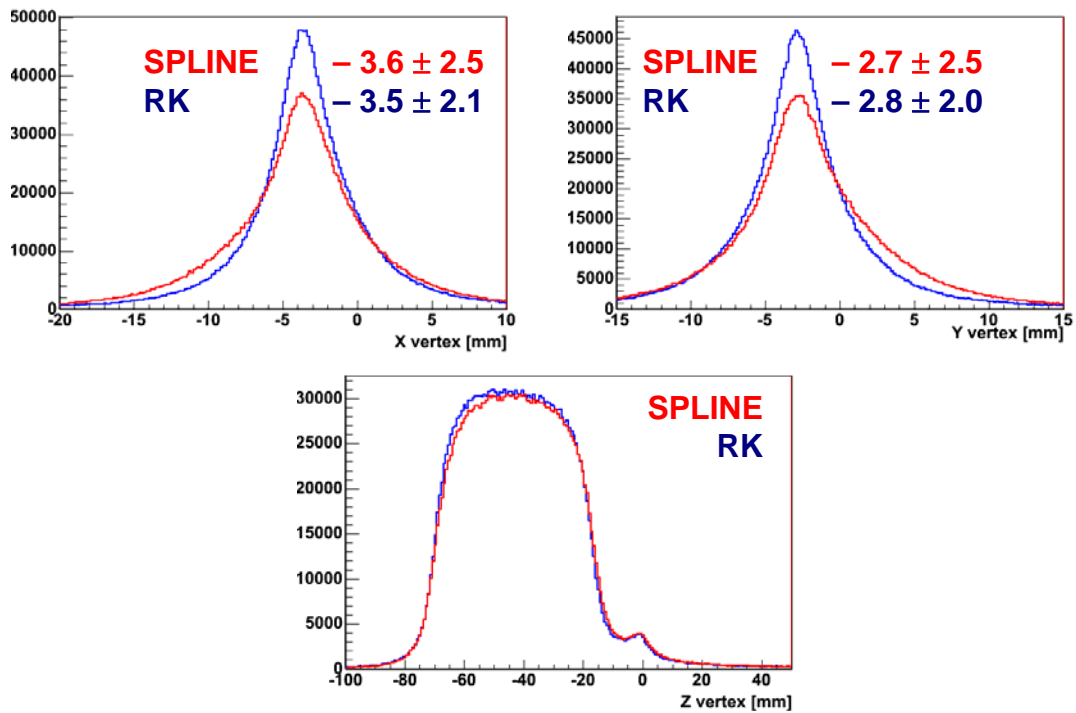


Figure 5.27 – Comparison of vertex coordinate distributions between Spline and Runge Kutta algorithms. While the z coordinate remains substantially unchanged, x and y are corrected toward the peak position. The distribution widths for Runge Kutta agree to what was obtained in no field data.

While the z coordinate remains almost unchanged, a strong improvement can be seen in x and y distributions. In this case the peak positions remain unchanged, while the distributions become narrower, with widths close to the values obtained in no field data.

We can argue Runge Kutta algorithm applies a strong correction on the track variables, and the improvements is visible at the level of vertex reconstruction. In the following paragraphs results on angular distributions will be shown.

5.6.2 Azimuthal angle

In order to understand the changes done by the Runge Kutta algorithm, we can look to distributions of the difference between the segment value of azimuthal angle ϕ and the new one recalculated by Runge Kutta tracking.

By looking into Figure 5.28, which shows the ϕ deviations made by Runge Kutta respect to MDC segment values, the azimuthal angle was changed mostly in the low polar angle region (right plot), where momentum resolution distributions for Spline showed some irregularities, while deviations in function of azimuthal angle are not so strong. It seems Runge Kutta algorithm is able to improve the alignment, by moving track parameters in the “correct” position; we have to stress that Runge Kutta tracking code does not use elastic scattering information but only the particle equation of motion inside magnetic field, so the algorithm is substantially independent from the studied physical process.

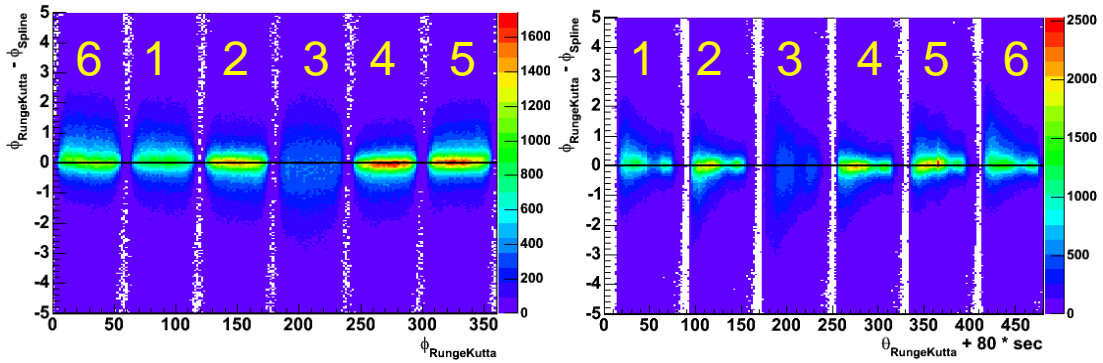


Figure 5.28 – Differences between the azimuthal values obtained by spline tracks (MDC segment values) and the recalculated Runge Kutta ones, in function of ϕ (left) and θ (right).

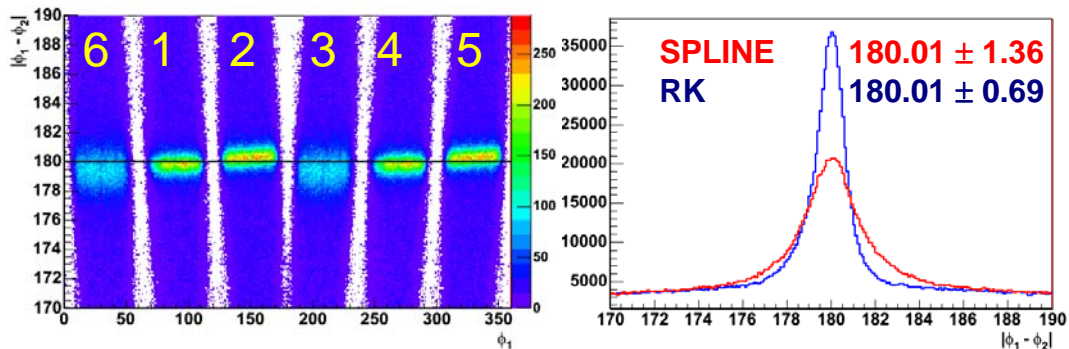


Figure 5.29 – Coplanarity plots for azimuthal angles obtained by Runge Kutta tracking. On the left the distribution in function of ϕ value of one proton, on the right comparison between $|\phi_1 - \phi_2|$ peak obtained by Spline and the corrected by Runge Kutta. The improvement is quite impressive.

Coplanarity distributions after the adjustment are shown in Figure 5.29. The azimuthal resolution improved a lot, and in this case we can see some small systematic deviations which are still present. Nevertheless, by looking into one dimensional spectrum (right side), the obtained angular resolution has improved of about a factor 2, and the value is in agreement to the one found in no field data (0.78° for inner MDC segments)

We can argue Runge Kutta recalculates azimuthal angles by correcting segment values, in order to get rid of eventual alignment problems and of the presence of a low field inside inner MDC chambers.

5.6.3 Polar angle

The same analysis can be done for θ polar angle. In Figure 5.30 it is possible to see polar angle deviations plotted in function of ϕ and θ .

By looking at the distribution in function of the azimuthal angle, while at the chamber centres the ϕ value is almost good, at the edges the reconstructed value is lower than what obtained by the segment. We can see MDC tracking has some problem in the not central region of the chambers; this could be connected to alignment, but we

must consider the edges of MDC modules are closer to magnet coils, and there the magnetic field is stronger respect to central regions, so the particle trajectory can be affected by the field. Nevertheless Runge Kutta tracking can recover this effect, taking into account the field effect inside chambers.

By checking deviations in function of polar angle θ , the patterns show adjustments were done for each sector in a different way.

In Figure 5.31 the distribution of the new $\tan\theta_1 \cdot \tan\theta_2$ value is shown, in comparison to the Spline one. The position of the peak remains almost unchanged, while the width is reduced to lower values, even if still higher respect to the no field numbers.

By checking the tangents product in function of θ (Figure 5.32), the distribution is well centred at the kinematical prediction, while the width has a small improvement respect to the previous values, which can be checked by simply looking at the scale of z axis (the sample of analysed pairs is the same used for spline analysis).

The obtained resolution is about 1.2%, in comparison with 0.9% obtained with no field data from inner segment.

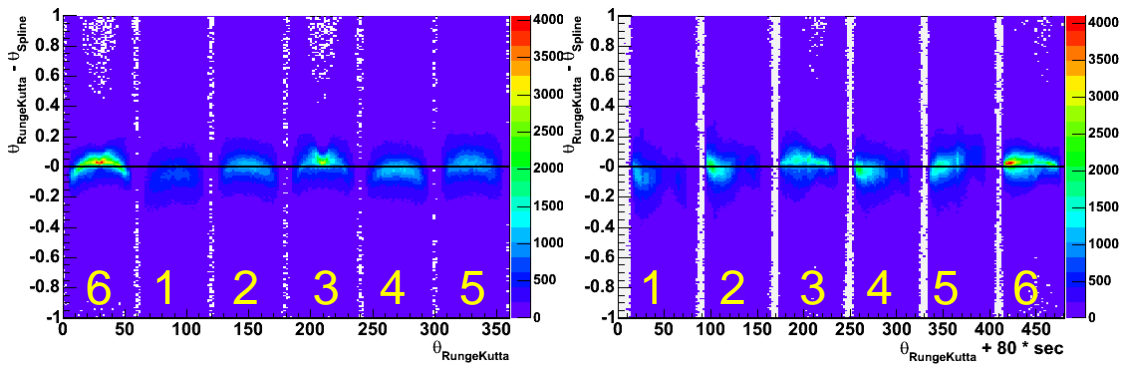


Figure 5.30 - Difference between polar angles obtained by spline tracks and the recalculated Runge Kutta values, in function of ϕ and θ . We can see the changes occur mostly at the edges on the chambers.

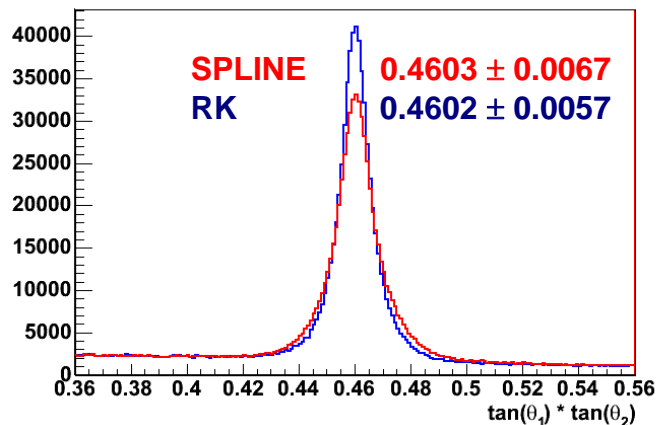


Figure 5.31 – Comparison between $\tan\theta_1 \cdot \tan\theta_2$ distributions for spline and Runge-Kutta algorithms. Even in this case an improvement is visible, but not so strong as for azimuthal angles.

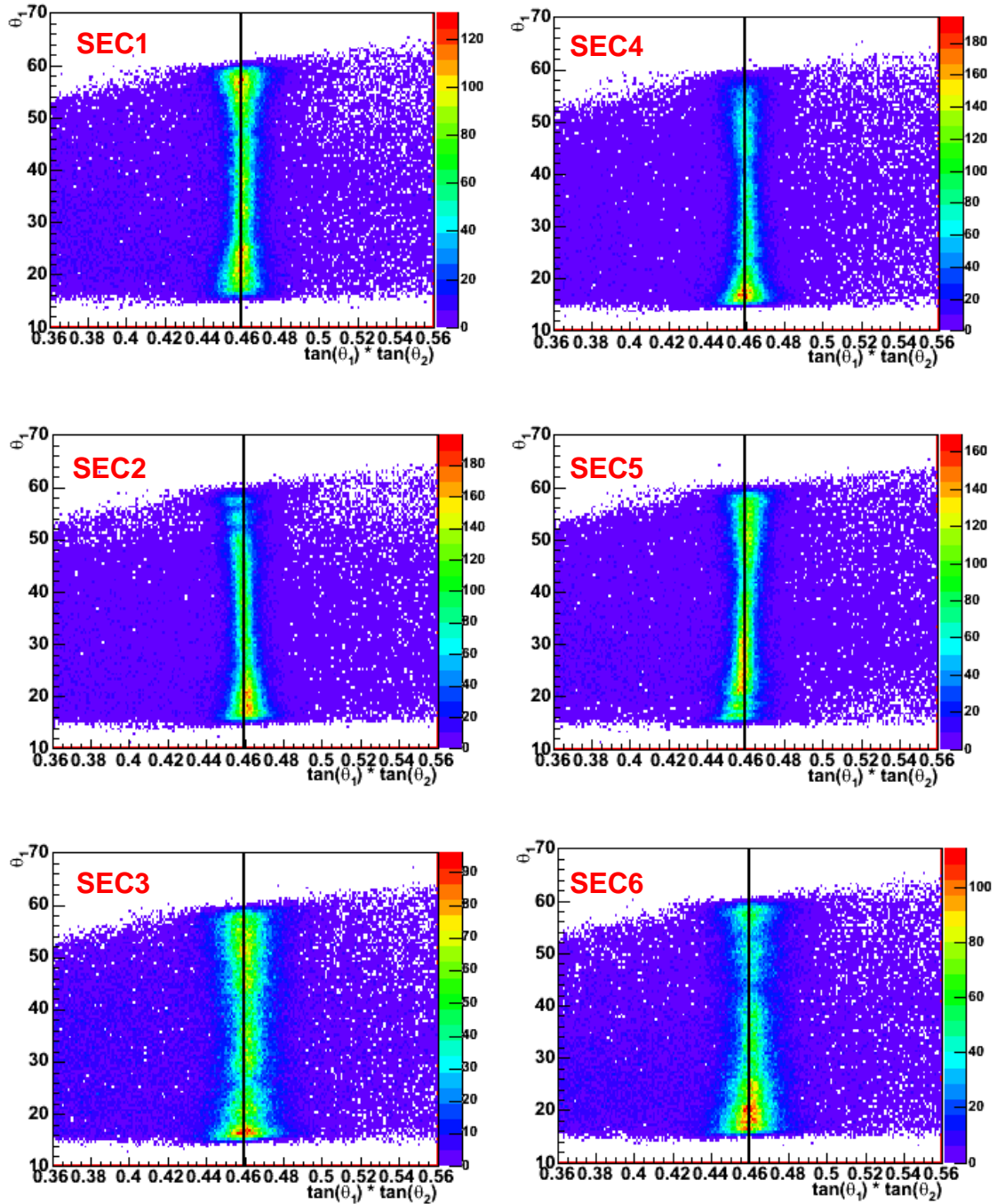


Figure 5.32 - Plots for θ_1 versus $\tan\theta_1 \cdot \tan\theta_2$ by using Runge Kutta recalculated polar angles. As expected the distributions show an improvement respect to MDC values (Figure 5.19), and they are better centred to the kinematical prediction (black lines).

5.6.4 Elastic selection

By using Runge Kutta angular values we are able to construct a χ^2 function such as 5-22, but this time using the values obtained by fits over Runge Kutta variables.

The χ distribution is shown in Figure 5.33, and it is similar to what obtained using Spline tracking.

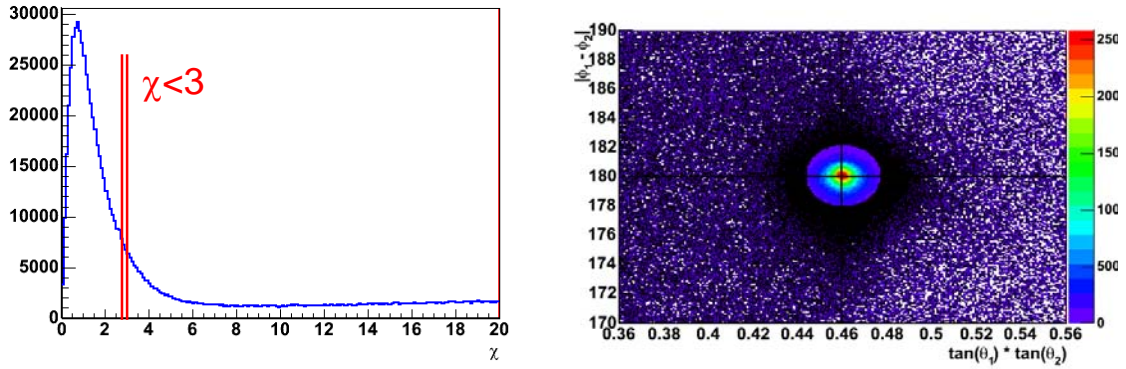


Figure 5.33 - χ distribution for elastic pairs using Runge Kutta tracking (left side). On right side the elastic topologic spectrum is shown after the cut $\chi < 3$; the black dots correspond to rejected pairs.

In order to compare the same data sample it was used the same cut to do a topologic selection on elastic pairs, so a condition on $\chi < 3$ was imposed.

The right side of Figure 5.33 shows the topologic distribution after the selection. We can see the peak is narrower respect to the Spline one, so in this case we are cutting away much more background coming from not elastic processes.

After applying the χ selection, we can study elastic pairs and evaluate momentum reconstruction resolution as already shown before for Spline.

5.6.5 Momentum reconstruction

By comparing the Runge Kutta momentum value with the theoretical one calculated using the reconstructed polar angle θ , we can evaluate the momentum resolution of the algorithm.

In Figure 5.34 the ratio between experimental values and theoretical ones is plotted in function of the polar angle θ .

Respect to spline tracking the distributions so obtained are much better centred to the correct value, and they show a lower spread. By looking at lower polar angle values some deviations are still present, but they are decreased by the Runge Kutta angular adjustment. We can argue the alignment needs an improvement, but nevertheless the Runge Kutta tracking algorithm is able to recover the errors made by a not exact position determination in the laboratory coordinate system.

The obtained resolution plots are shown in Figure 5.35, in comparison for different tracking systems.

Three MDC sectors do not show strong effects after the recalculation, considering that the peak position and the widths remain almost the same as before. Sector 6 remains unchanged, while in sector 3 the resolution is worse of one point percent. We can state at the moment Runge Kutta tracking does not improve the measure when only 3 planes are present, because of the lower number of points usable for the reconstruction (Runge Kutta tracking does not use kickplane points).

By checking 4MDC sectors the improvement in terms of resolution is strong. All the resolution values in these sectors decrease and even the peak position is better centred to the value “one” (1). The improvement is much stronger for sector 1, which showed a worse Spline resolution respect to the others, mainly connected to the lesser number of working wire layers respect to other sectors. Even in this case Runge Kutta tracking can recover the loss in resolution connected to the lack of wires, by combining

the values we can get from all the wire layers which are present in the same sectors (inner and outer).

The sector which present the best momentum reconstruction is number 2, with a resolution of 4.0%, compared to the 4.8% from the spline algorithm.

If we check the plots of Figure 5.36 the difference between reconstructed and theoretical momentum values is reduced respect to the Spline plots (Figure 5.24).

The last thing to check is the invariant mass resolution we can get by using this angular and momentum reconstruction. Figure 5.37 shows invariant mass plots for different sector pairs, compared to the distributions using spline momenta.

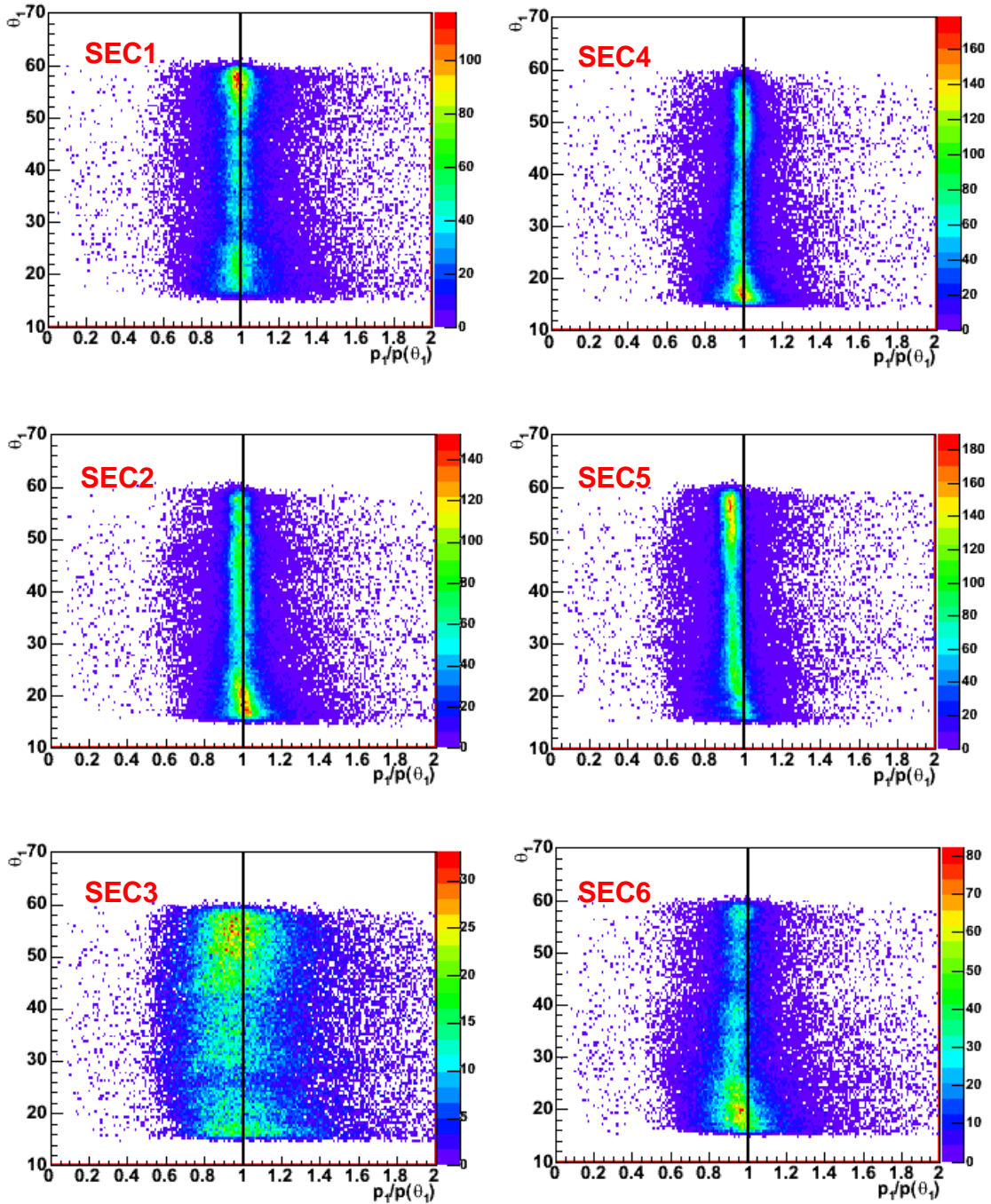


Figure 5.34– Ratios between reconstructed and kinematical momentum for Runge Kutta tracking algorithm, in function of polar angle. The improvement respect to spline distributions (Figure 5.23) is well visible.

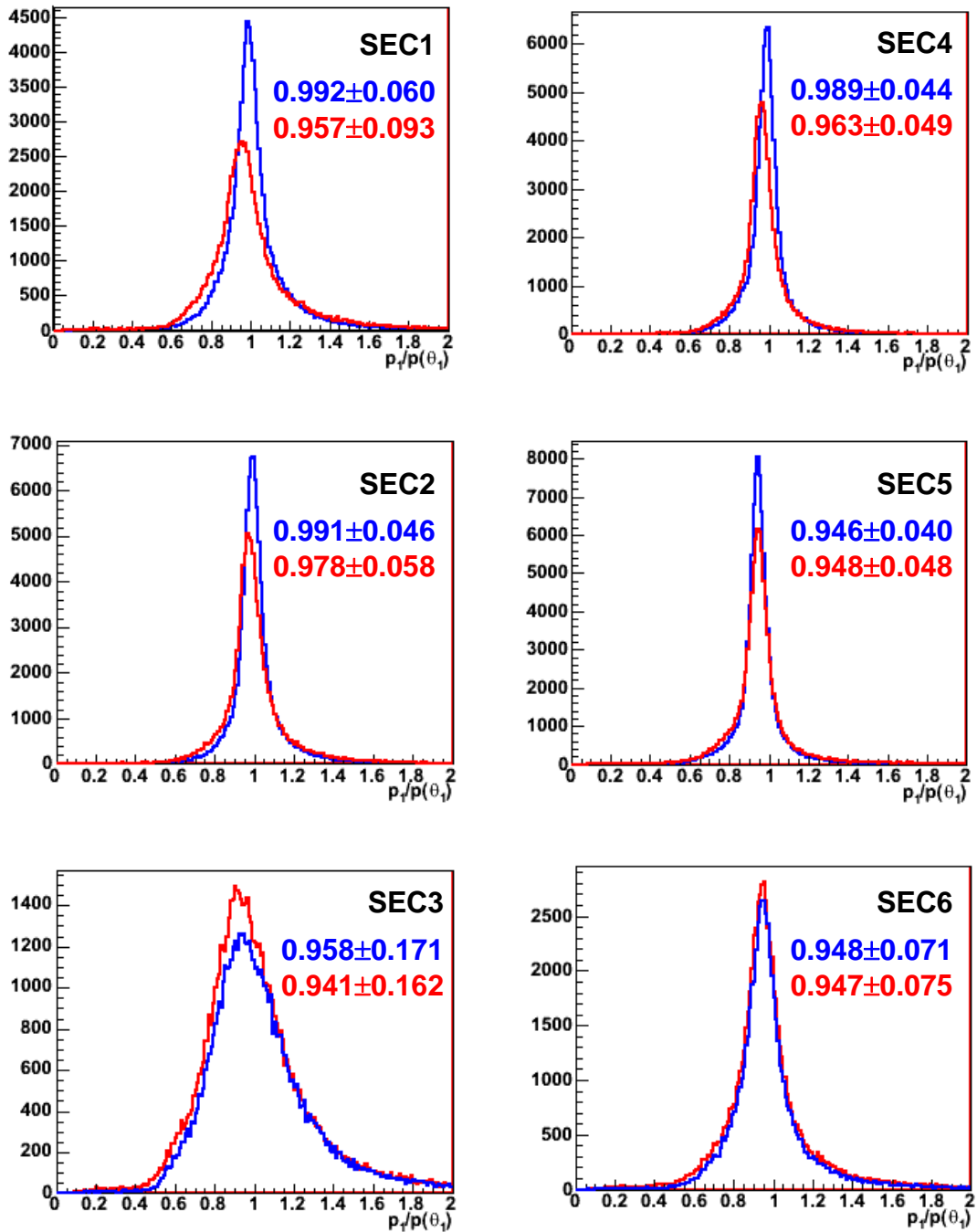


Figure 5.35– Ratios between reconstructed momentum and kinematical prediction from polar angle θ , obtained by using Runge Kutta (in blue) and Spline (in red) tracking algorithms.

The improvement in resolution is well visible, in particular in the region of central polar angles (right plots), where the discrepancy present in spline is lowered and the distribution is moved toward the theoretical value.

The best invariant mass resolution value is 2.3% at 2.7 GeV/c², for 2-5 sector pair. For 3MDC sectors the resolution stays at 6%, but we have to underline this high value is mainly connected to the poor resolution in sector 3, due to the lack of wire layers.

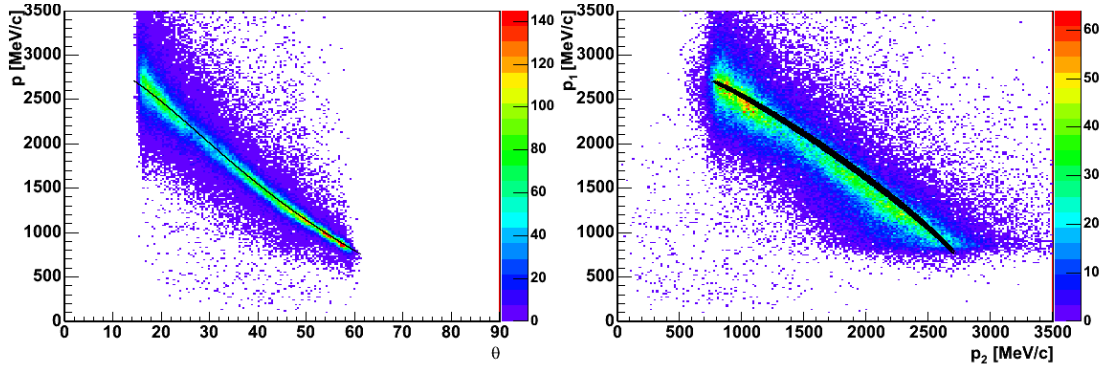


Figure 5.36 – Momentum plots for sector pair 1-4, which shows a better resolution. Momentum versus polar angle (right side), and momentum of a proton respect to the momentum of the other one (left side). The black lines represent theoretical predictions.

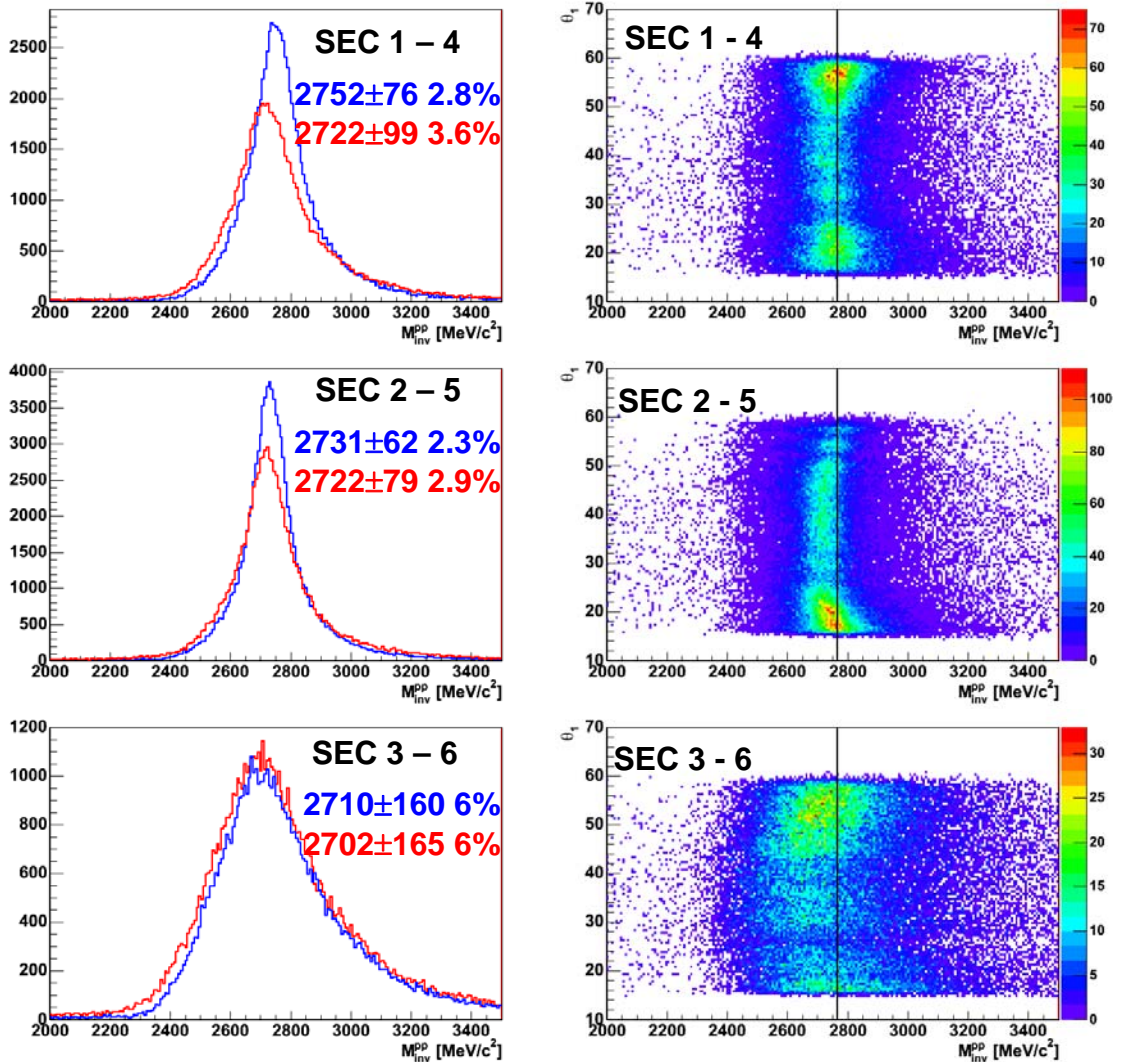


Figure 5.37 – Missing mass distributions for Runge Kutta tracking (in blue) compared to Spline one (in red). The RK mass distribution in function of polar angle of one proton on the right. The kinematical value of proton-proton invariant mass is $2768 \text{ MeV}/c^2$, and it is indicated by the black lines.

5.7 Momentum resolution summary

All the momentum resolution values obtained for Spline and Runge Kutta algorithms are reported in Table 5-2, together with the values from simulation analysis by using exactly the same procedure to select protons from elastic scattering. **Errore. L'origine riferimento non è stata trovata.** shows the obtained values for invariant mass resolution of elastic pairs.

The discrepancy between simulation values and experimental ones is actually under study. The simulation takes into account the number of working layers for each MDC chamber as present during data acquisition, and this feature can be seen in the differences between resolution values for different sectors, which follow the same behaviours of experimental data. Moreover in simulation the geometry of the various sub detectors is known so effects of misalignment are not present.

Nevertheless actually the simulation setup differs from the experiment. First of all in simulation the beam is centred at (0,0) position, while it was found in the vertex reconstruction analysis that during the acquisition time the beam was shifted and even moved during the days. This shift imposes a global movement of the “real” coordinate system respect to the “laboratory” one, which is calculated by the alignment procedure.

While this effect is of a secondary order, there are some hints that the beam was not parallel to the ground level but a bit tilted respect to z axis; all the angular reconstructed variables could be affected by this effect, and in particular the expectation value of momentum calculated by polar angle. In this case by correcting the geometry definition it will be possible to have better resolution values. So we can state at the moment the obtained values are an upper limit of the HADES momentum resolution.

Moreover the effects of a drift times measured in absence of the START detector, and of a possible inner misalignment of wire layers, are at the moment under study and their relative loss in resolution.

However, by analysing elastic scattering process, for the first time it was possible to evaluate the experimental angular and momentum resolution of the HADES tracking system, to understand possible problems and the manners how to solve them. This was one of the main goal of the January 2004 experiment.

The second goal was the exclusive η reconstruction, and in chapter XX it will be shown it is possible with the current setup and tracking resolution.

Sector		1	2	3	4	5	6
Spline	SIM	2.1 %	1.9 %	3.4 %	2.0 %	1.8 %	2.4 %
	EXP	9.3 %	5.8 %	16.2 %	4.9 %	4.8 %	7.5 %
RK	SIM	1.4 %	1.2 %	2.7 %	1.4 %	1.6 %	2.0 %
	EXP	6.0 %	4.6 %	17.1 %	4.4 %	4.1 %	7.1 %

Table 5-2 - Values of momentum resolution for Spline and Runge Kutta tracking algorithms, for simulation data and experimental ones.

Sector pair			1-4	2-5	3-6
Spline	SIM	Mass [MeV/c ²]	2760	2758	2759
		σ [MeV/c ²]	21	20	31
		dM/M [%]	0.77	0.73	1.11
	EXP	Mass [MeV/c ²]	2722	2722	2702
		σ [MeV/c ²]	99	79	165
		dM/M [%]	3.6	2.9	6.1
RK	SIM	Mass [MeV/c ²]	2764	2764	2763
		σ [MeV/c ²]	16	15	27
		dM/M [%]	0.6	0.6	1.0
	EXP	Mass [MeV/c ²]	2752	2731	2710
		σ [MeV/c ²]	76	62	160
		dM/M [%]	2.8	2.3	5.9

Table 5-3 - Values of invariant mass resolution for Spline and Runge Kutta tracking algorithms, for simulation data and experimental ones.

NOTE

Spline tracking: equazione 5-11 due volte
Runge-Kutta tracking: equazione 5-14, equazione 5-16
Elastic selection: equazione 5-22
Momentum resolution summary: capitolo XX per eta reconstruction

5	Tracking and alignment	1
5.1	Elastic kinematics	1
5.2	Alignment strategy.....	3
5.3	Tracking algorithms	6
5.3.1	Kickplane	6
5.3.2	Spline tracking	8
5.3.3	Runge-Kutta tracking.....	10
5.4	No Field runs.....	11
5.4.1	Vertex reconstruction.....	12
5.4.2	Azimuthal angle	14
5.4.3	Polar angle	17
5.5	Field data – Spline Tracking.....	19
5.5.1	Vertex reconstruction.....	20
5.5.2	Azimuthal angle	21
5.5.3	Polar angle	21
5.5.4	Elastic selection	23
5.5.5	Momentum reconstruction	24
5.6	Field Data – Runge Kutta Tracking.....	28
5.6.1	Vertex reconstruction.....	28
5.6.2	Azimuthal angle	29
5.6.3	Polar angle	30
5.6.4	Elastic selection	32
5.6.5	Momentum reconstruction	33
5.7	Momentum resolution summary	37